Advancing Energy Systems with *In-Situ* and *Operando* Surface-Enhanced Raman Scattering Spectroscopy

Haoming Bao,[1,2‡] Shi Xuan Leong,[1,2‡] Jaslyn Ru Ting Chen,[2] Zhenhai Shi,[1] Suli Chen,[1] Yan Lv,[1] Tianxi Liu,[1] In Yee Phang[1] and Xing Yi Ling*[1,2]*

[1] Key Laboratory of Synthetic and Biological Colloids, Ministry of Education, International Joint Research Laboratory for Nano Energy Composites, School of Chemical and Material Engineering, Jiangnan University, Wuxi.

[2] School of Chemistry, Chemical Engineering and Biotechnology, Nanyang Technological University, 21 Nanyang Link.

‡ These authors contributed equally.

* To whom all correspondence should be addressed.

E-mail: xyling@ntu.edu.sg, yanlv@jiangnan.edu.cn

Abstract

Surface-enhanced Raman scattering spectroscopy (SERS) has emerged as a powerful analytical technique to enable nanoscale investigations of energy systems. This mini-review focuses on the applications of *in-situ* and *operando* SERS in energy-related research, highlighting its unique capabilities and significant contributions to understanding energy storage and conversion processes. We first introduce the fundamental principles of SERS, key SERS-derived techniques, and commonly employed platforms. Subsequently, we delve into the diverse applications of *in-situ* and *operando* SERS across various energy systems, encompassing photocatalytic and electrocatalytic systems, fuel cells, solar cells, and batteries. Finally, we conclude with our perspective on the current challenges and prospects in this area. We hope this mini-review serves as an essential overview to guide the design and implementation of *in-situ* and *operando* SERS studies of energy systems.

Keywords: Surface-enhanced Raman scattering spectroscopy (SERS), *In-situ*, *Operando*, Energy systems, Photocatalysis, Electrocatalysis, Fuel Cells, Solar Cells, Batteries

Introduction

The development of advanced energy storage and conversion systems with higher efficiency, durability, and safety is critical to transit away from our current over-reliance on fossil fuels and effectively combat the ongoing energy crisis.[1, 2] The urgency for these advancements is underscored by the 'Net-Zero by 2050' Roadmap released by the International Energy Agency (IEA) in 2021, which positions the accelerated growth of sustainable, renewable energy storage technologies among its key global technological agendas. Among various energy systems, photocatalytic and electrocatalytic systems, fuel cells, solar cells, and batteries play pivotal roles in meeting these needs. Despite the significant progress to date, these energy systems still need to be significantly improved to cater to the ever-growing demand. Key issues include, but are not limited to, maximizing energy storage densities in batteries, achieving high faradaic efficiencies, selectivities and preventing catalyst failure in fuel cells and electrocatalytic systems, as well as enhancing long-term stability and photoconversion efficiencies in solar cells and photocatalytic systems. Fundamentally, the rational design of better catalysts, reactors, and interfaces across various energy systems is impeded by the lack of near-total mechanistic understanding. However, such near-total mechanistic understanding remains challenging due to the high complexity of energy systems, which involves interrelated dynamic processes such as charge transfer, evolution of transient species, and surface/interface compositional and structural changes.

To address this challenge, the strategic use of *in-situ* or *operando* techniques offers a powerful toolkit for real-time tracking of these dynamic processes with high sensitivity and excellent spatiotemporal resolution.[3-8] By definition, *in-situ* measurements are performed on-

site in their native working environments, while *operando* studies focus on the real-time and dynamic analysis of the system during its active operation.[9, 10] Nevertheless, as most research employs these terms interchangeably, we will directly use the terms defined in each case study in the subsequent sections. Currently, diverse *in-situ*/*operando* techniques have been leveraged to capitalize on their unique technological advantages to probe different aspects of energy systems.[3-8] For example, techniques such as transmission electron microscopy (TEM), X-ray diffraction (XRD), and X-ray absorption spectroscopy (XAS) are highly useful for *in-situ* analysis of structural evolution in crystallographic structures, crystal defects, and chemical coordination information.[3-5, 7, 8] On the other hand, techniques such as atomic force microscopy (AFM), scanning tunneling microscope (STM), and X-ray photoelectron spectroscopy (XPS) can provide essential surface information in terms of changes in topography or chemical states.[3, 5-7] As for vibrational spectroscopic techniques such as surface-enhanced Raman scattering spectroscopy (SERS) and infrared spectroscopy (IR), they offer valuable, molecular-level insights into structure-activity correlations, reaction pathways, and key surface/interfacial dynamic events during reactions, which can guide the development of novel and high-performance energy-related materials.[11-16] Among these techniques, SERS stands out as a powerful tool which provides high molecular sensitivity and vibrational fingerprinting capability by amplifying the weak intrinsic Raman spectra of molecules adsorbed or close to nanostructured metal/semiconductor surfaces by $>10^{10}$-fold.[11-16] At the same time, SERS has excellent compatibility with both air and aqueous environments, making it particularly suited for *in-situ*/*operando* studies of most energy systems.

In this mini-review, we offer a critical outlook on the use of *in-situ*/*operando* SERS to

elucidate nanoscale energy storage and conversion processes in various energy systems, spanning photocatalytic and electrocatalytic energy systems, fuel cells, solar cells, and batteries. To guide readers on how to leverage SERS for energy-related investigations, we first introduce the fundamental principles of SERS and discuss key techniques and platform design configurations that can be integrated with *in-situ/operando* SERS measurements. Next, for each energy system of interest, we systematically highlight the current state-of-the-art in utilizing *in-situ/operando* SERS to derive mechanistic insights that were previously elusive or ambiguous, using representative works from 2018 to 2023. We focus on three main aspects: (i) investigation of structure-activity correlations, such as surface crystallinity and molecular arrangements, (ii) elucidation of reaction pathways by tracking species evolution, and (iii) monitoring of other surface/interfacial events, such as charge transfer and catalyst surface reconstruction. Finally, we conclude with our perspective on the current challenges and potential research directions to further leverage *in-situ*/*operando* SERS for accelerating the development of next-generation energy technologies.

Background on SERS

To facilitate readers in understanding the significance of *in-situ*/*operando* SERS for energy systems and its implementation, we first provide an overview of SERS, introducing its fundamental working principles and commonly employed platform configurations. We also highlight a key variant of the SERS technique, namely tip-enhanced Raman spectroscopy (TERS), which demonstrates immense potential for *in-situ/operando* investigations in energy systems.

Working principles of SERS

SERS is a vibrational spectroscopic technique in which the inelastic Raman scattering of incident photons by molecules is amplified by factors up to 10^{12} or larger when the molecules are adsorbed on or close to nanostructured metal/semiconductor surfaces.[11-16] It is widely accepted that the Raman signal enhancement in SERS can be attributed to two key mechanisms, namely the electromagnetic enhancement (EM) and the chemical enhancement (CHEM) (Figure 1A).

EM arises from a unique phenomenon known as localized surface plasmon resonance (LSPR), which relies on the resonance between the incident light and collective electron oscillations of the plasmonic nanomaterial (usually metallic) upon laser irradiation (Figure 1A-i).[17] The LSPR excitation in turn creates a localized region of highly intense electromagnetic field near the metal surface at distances < 10 nm where both the incident and scattered light are amplified, contributing to a large Raman signal enhancement of up to 10^{12}.[11-16] The magnitude of EM enhancement depends on various factors including the nanomaterial (Au, Ag, Cu, *etc.*), size, morphology, and inter-particle gap.

On the other hand, CHEM involves the photon-induced charge transfer (CT) between the substrate (semiconductors or metals) and chemisorbed molecules (Figure 1A-ii).[18, 19] Resonance-like Raman scattering is produced when the photon energy of the incident laser matches the CT transition energy between the molecule and the substrate, which increases the adsorbed molecule's polarizability to effect Raman signal enhancement of about 10^2. Collectively, the combined effect of EM and CHEM mechanisms is essential for SERS to achieve high molecular sensitivity. Readers interested in the fundamental, detailed explanations

of the physics behind SERS can refer to these comprehensive reviews.[20, 21]

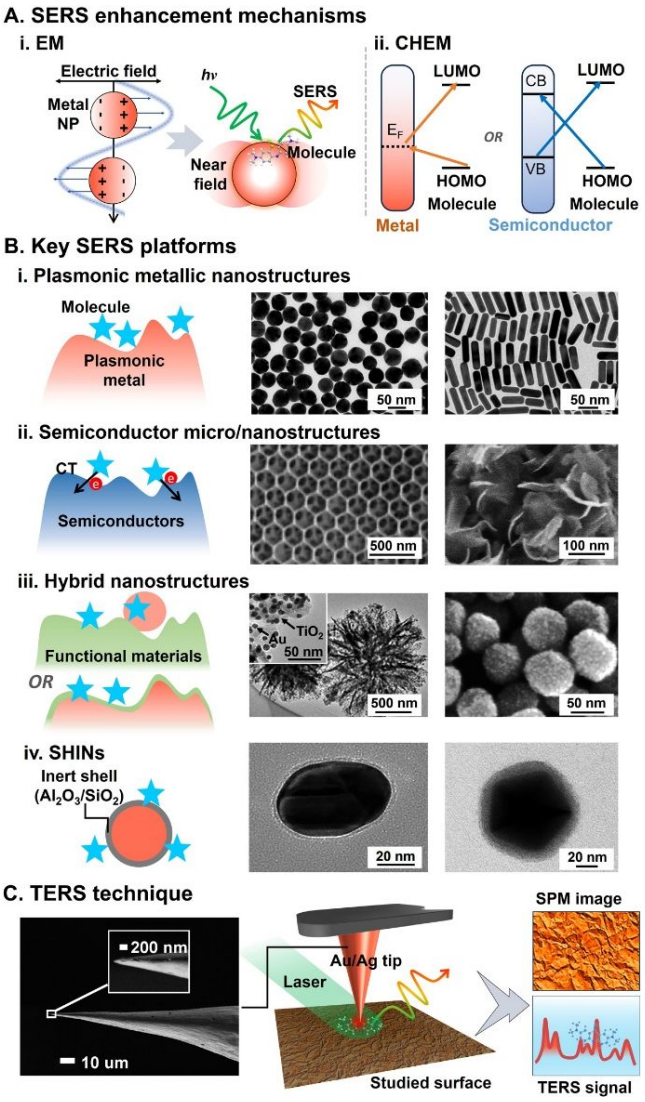

Figure 1. **Introduction of SERS.** (A) Schematics of SERS working principles, namely (i) EM and (ii) CHEM. (B) Representative SERS platforms. (i) Plasmonic metallic nanostructures, with TEM images of Au NPs (left) and Ag nanorods (right). (ii) Semiconductor micro/nanostructures, with SEM images of reverse opal TiO_2 (left) and O-doped MoS_2 nanocrystals (right). (iii) Hybrid nanostructures, with TEM/SEM images of Au NP-decorated TiO_2 nanoflowers (left, the inset shows the magnified image) and Au@Pt NPs (right). (iv) SHINs, with TEM images of an isolated $Au@SiO_2$ NP with a near-spherical (left) and polyhedral (right) core. (C) Schematic of TERS technique. The SEM images and their insets show a typical tip for TERS. Reprinted and adapted with permission from (B) Refs. 22, 23, 24, 25, 26, 27, 28, 29, and (C) ref. 30. Copyright 2006-2008, 2015-2018, 2022 American Chemical Society. Copyright 2017 Zuhui Zheng, Shan Cong, Wenbin Gong, Jinnan Xuan, Guohui Li, Weibang Lu, Fengxia Geng & Zhigang Zhao.

Commonly employed SERS platforms

In terms of SERS platforms, most utilize plasmonic metallic nanomaterials (Au, Ag, Cu etc.) due to their strong LSPRs that ensure high SERS EM enhancement.[21-23, 31] To further maximize SERS signals, these platforms possess nanoscale surface roughness, which include nanoparticles (NPs) and various shape-controlled nanostructures with large curvatures and/or sharp tips and edges, such as nanocubes, nanorods, and nanostars (Figure 1B-i). Moreover, these NPs and nanostructures can also be organized into 2D and 3D assemblies to achieve heightened SERS enhancements *via* inter-particle plasmonic coupling.[32-38] In addition to plasmonic metallic nanostructures, nano-architectured semiconductor materials such as Cu_2O, TiO_2, ZnO, and MoS_2 can also serve as SERS-active platforms.[24, 25, 39-41] For these semiconductor-based platforms, CHEM arising from charge transfer (CT) between the semiconductor material and the adsorbed molecules is the primary enhancement mechanism (Figure 1B-ii). Target nanostructures employed in various energy systems that are fabricated from these SERS-active materials can thus be directly employed for *in-situ/operando* SERS studies. It is noteworthy that compared to plasmonic metal-based platforms in which EM enhancement is stronger than CHEM enhancement, semiconductor-based platforms are inherently well-suited for studying CT processes in energy systems since CT is the main source of their SERS effect.

To obtain *in-situ*/*operando* spectroscopic insights on non-SERS active functional materials, researchers have developed various hybrid configurations which integrate these functional surfaces with plasmonic materials. Notable hybrid configurations include core@shell, core-satellites, and other hybrid nanostructures in which the functional materials

are encapsulated over plasmonic metal cores, and incorporated as satellite nanostructures, respectively (Figure 1B-iii).[14, 26, 27, 42-45] In these hybrid configurations, the Raman signals from chemical species on these functional materials are effectively amplified by EM enhancement from the SERS-active plasmonic cores. They thus offer a generic substrate architecture with additional versatility to monitor various catalytic and other surface processes on a wide range of target surfaces.

Another widely used platform configuration in energy system study is shell-isolated nanoparticles (SHINs), in which a plasmonic core is surrounded with an ultrathin inert dielectric shell of SiO_2 or Al_2O_3 (Figure 1B-iv).[28, 29, 46, 47] Non-SERS active materials of interest can be loaded onto these SHINs in SHIN-satellites configurations for *in-situ/operando* SERS studies. Moreover, in specific cases where atomically flat single crystalline surfaces are preferred as model energy systems, e.g., for fundamental investigations, SHINs can be assembled on the material surface to amplify the Raman signals of adsorbed species. SERS measurements performed with SHINs is conventionally referred to as shell-isolated nanoparticle-enhanced Raman spectroscopy (SHINERS).[28, 29, 46, 47] Notably, the inert shell prevents the direct adsorption of target molecules on the plasmonic Au or Ag cores to avoid potential undesired catalysis (such as electrocatalytic oxygen reduction reaction, ORR) which may interfere with the *in-situ*/*operando* measurements. On the other hand, a sufficiently thin (< 5 nm) inert shell is critical to maintain satisfactory SERS enhancement. The shell also enhances the thermal and chemical stability of the plasmonic cores, which facilitates SERS exploration in energy systems with harsher system conditions such as high temperatures or highly acidic chemical

environments. Readers interested in the more details about SHINERS can refer to the primer paper.[48]

In overall, SERS thus offers high molecular sensitivity and vibrational fingerprinting capability for univocal molecular identification, making it highly suited to acquire molecular-level insights on dynamic energy storage and conversion processes in energy systems. Nonetheless, since SERS requires roughened or nanostructured surfaces, it is incompatible with smooth material surfaces, which could limit its application in cases where atomically flat surfaces are favored as model energy systems. In addition, the submicron spatial resolution of SERS may be insufficient to capture spectroscopic evidence of position-dependent events such as surface reconstruction.

Tip-enhanced Raman spectroscopy (TERS)

To circumvent these limitations and probe dynamic surface/interfacial events with high spatial resolutions, SERS can be integrated with a scanning probe system. Conventionally referred to as tip-enhanced Raman spectroscopy (TERS), this alternative detection modality locally amplifies the EM field at a plasmonic tip (Figure 1C).[30, 49-51] TERS allows effective molecular detection even on atomically flat single crystal surfaces, which improves the morphological generality of SERS to better probe surface/interfacial processes across a broader range of materials and surfaces. Next, it provides high spatial resolution for atomic-level measurements with precise positioning, which is highly relevant to obtain nanoscale molecular and topographical information in energy systems, such as identifying positions of active sites or probing heterogeneous surfaces.[30, 49-51] For more in-depth explanations on TERS, we recommend this review.[52]

In overall, the continuous development of SERS offers researchers powerful tools to unravel various mechanistic insights in diverse energy systems, including photocatalytic and electrocatalytic systems, fuel cells, solar cells, and batteries, which will be discussed in the following section. To provide strategic guidance for readers in their preliminary platform selection for *in-situ/operando* SERS investigations in energy systems, we consolidate the main features and advantages of these platform configurations in Table 1.

Table 1. Overview of commonly employed SERS platform configurations.

Platforms	Description	Examples	Advantages	Ref.
Plasmonic metallic nanostructures	Support strong LSPRs in the visible light to near-infrared region	Au NPs Ag nanocubes Au nanorods	• High molecular sensitivity • Can be functionalized with additional probe molecules to track species of low Raman cross-sections/are poorly adsorbing	11-16, 21-23, 31-38
Semiconductor nanostructures	Semiconductor materials that utilize CHEM as the main SERS enhancement mechanism	Cu_2O superstructures TiO_2 inverse opals ZnO nanocages	• Suitable to study CT processes • Low cost	18, 19, 24, 25, 39-41
Functional-material/plasmonic-metal hybrid nanostructures	Core@shell: functional material of interest (usually non-SERS active) encapsulating plasmonic metal cores. Core-satellites: functional material of interest (usually non-SERS active) integrated as satellites on a plasmonic metal core.	Au@Pt NPs Ag NP-decorated ZnO nanorod array Au core-metal oxide satellite nanostructures	• Enable SERS investigations on non-SERS active materials of interest	14, 26, 27, 42-45
Shell-isolated nanoparticles (SHINs)	Plasmonic core wrapped with an ultrathin inert dielectric shell (usually SiO_2 or Al_2O_3)	Au@SiO_2 NPs Au@Al_2O_3 NPs	• High thermal and chemical stability • Prevent interference from inner plasmonic core (e.g., undesirable photocatalysis) • Enable SERS investigations on non-SERS active materials of interest	28, 29, 46, 47, 53-59
Plasmonic tips for TERS	Standard tips coated with plasmonic metals (usually Ag or Au) OR Electrochemical etching of all-metal tips AND/OR Grafting of NPs at the metallic tips.		• High morphological generality and does not require target surfaces to possess nanoscale roughness • High spatial resolution with precise positioning	30, 49-51, 54

*Bimetallic nanostructures in which both metals act as the catalysts.

Applications of *in-situ*/*operando* SERS for energy systems

For each energy system, we present the commonly utilized *in-situ/operando* reaction-SERS setups, as well as the novel fundamental mechanistic insights gained in terms of structure-activity correlations, reaction pathways, and other surface/interfacial events and processes. We also provide a non-exhaustive summary of the latest developments in utilizing in-situ/operando SERS across different energy systems in Table 2.

Table 2. Current progress in utilizing *in-situ/operando* SERS across different energy systems.

Energy system	Studied issue	Phenomenon of interest	Platform/nanomaterial	Additional information	Ref.
Photocatalytic systems	Structure-activity correlations	Crystal defects such as oxygen vacancies	Au NPs on metal oxide films (TiO_2, ZnO and WO_3) and NPs (TiO_2)	*p*-mercaptobenzoic acid as probe molecules	60, 61
		Different crystal phases	4H Au nanoribbons, *fcc* Au nanowires, *fcc* Au nanorods	N.A.	62
		Hot electrons and holes	Au@TiO_2 NPs	*p*-aminothiophenol as probe molecule	63
		Adsorbate molecular ordering	Electrochemically etched Ag tips on single and polycrystalline Au	4-nitrobenzenethiol dimerization	64
	Reaction pathways	Silanol photooxidation	SHIN-CuO core-satellite nanostructures	N.A.	53
		CO_2 reduction	Ag NPs	Single NP-level SERS	65, 66
Electrocatalytic systems	Structure-activity correlations & reaction pathways	Reaction intermediates & *in-situ* dynamic surface restructuring	Au@Ni_3FeO_x core-satellite superstructures	Oxygen evolution reaction (OER)	67
			Cu electrodes	CO_2 reduction (CO_2RR)	68, 69
	Structure-activity correlations	*In-situ* structural transformations	Nanorod-like bismuth-based metal organic frameworks	Nitrogen reduction reaction (NRR)	70
			Mo_2C-MoO_x on carbon cloth	Hydrogen evolution reaction (HER)	71
	Reaction pathways	Product selectivity mechanisms	Nanoporous Ag coated with Pd/Cu	CO_2 reduction (CO_2RR)	72
			Ag nanocubes coated with oleylamine-functionalized zeolitic imidazolate framework	NRR vs. HER with 4-mercaptopyridine as probe	73
	Other surface/interfacial events	Molecular ordering of interfacial water	Au@SiO_2 SHINs on Pd(*hkl*) surfaces	HER	54

Table 2. Current progress in utilizing *in-situ/operando* SERS across different energy systems (continued)

Energy system	Studied issue	Phenomenon of interest	Platform/nanomaterial	Additional information	Ref.
Fuel cells	Structure-activity correlations & reaction pathways	Doping of different metals	Hybrid Au@PtNi NPs, Au@Pd@Pt NPs, Pt-based ternary alloys	Oxygen reduction reaction (ORR)	15, 54, 74
			PtRu bimetallic catalysts, Au@PtNi	Hydrogen oxidation reaction (HOR)	75, 76
		Structure ordering degree	AuCu bimetallic nanocatalysts	ORR	77
	Reaction pathways	Composition and evolution of intermediates	Au@Pt, Au@Co, and Au@PtCo core-shell NPs	ORR	78
			$Au@SiO_2$ SHINs on Pt(hkl) surfaces	ORR	55-57
	Other surface/ interfacial events	Catalyst poisoning events	$Ag@SiO_2$ SHINs on various SOFC cathodes and cathodes	N.A.	79, 80, 81
Solar cells	Other surface/ interfacial events	Photoinduced interfacial reactions	$Au@SiO_2$ SHINs on TiO_2(*hkl*) surfaces	Photoinduced behaviors of dye molecules in DSSCs	58, 82
		Charge transfer processes	Various DSSC systems (e.g., TiO_2@N719@Ag, ZnO-TiO_2/N_3/Ag)	N.A.	83-85
Batteries	Reaction pathways	Composition of reaction intermediates	Polycrystalline rough Au electrode	Lithium-oxygen batteries	86
			Nickel–cobalt–manganese oxide (NCM)@Li_2O cathodes	Initial-anode-free lithium battery	87
	Other surface/ interfacial events	Compositions and dynamics of electrolyte interphases	Au nanocubes on $LiNi_{0.33}Co_{0.33}Mn_{0.33}O_2$ (LNMC) cathode	Lithium ion batteries	88
			$Au@SiO_2$ SHINs on different electrodes (e.g., Sn, Si etc.)	Lithium ion batteries	59, 89
			Nanostructured Cu, $Au@SiO_2$ SHINs with Li deposits	Lithium ion batteries	90

In-situ/*operando* SERS in photocatalytic systems

As one of the promising technologies to tackle the current issues of energy shortage and environmental pollution, it is crucial to design photocatalysts with enhanced solar energy conversion efficiencies and photocatalytic activities. The most common approach to set up an *in-situ/operando* SERS study of photocatalytic systems is to deposit the photocatalysts onto solid support substrates and subsequently obtain the SERS spectra using the same laser employed to initiate photocatalysis or an additional light source (Figure 2A-i).[53, 60, 62, 63] For real-time monitoring in liquid systems, the as-prepared substrates can be immobilized within microfluidic cells and then mounted on an inverted optical microscope system to allow the solution containing the target reactants to flow over the affixed photocatalysts (Figure 2A-ii).[65, 66] In addition, to prepare the photocatalysts for *in-situ/operando* SERS measurements, SERS-active photocatalysts such as Au nanowires and Ag NPs can be directly employed, while non-SERS active photocatalysts can be loaded onto plasmonic nanostructures or SHINs.[62, 65, 66]

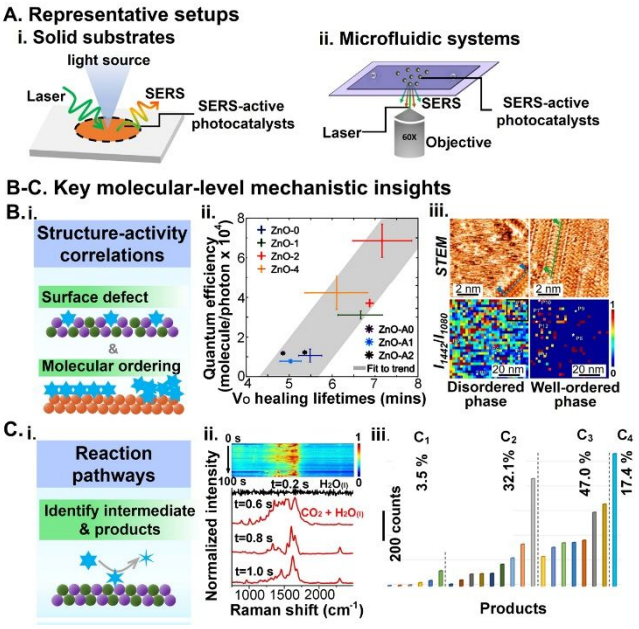

Figure 2. *In-situ*/*operando* SERS in photocatalytic systems. (A) Schematic of representative *in-situ/operando* SERS setups for photocatalytic systems, namely (i) direct dropcast on solid substrates and (ii) microfluidic systems. (B)(i) SERS for structure-activity correlations. (ii) Calculated V_O healing lifetimes determined from *in-situ* SERS spectra against the photocatalytic activity of ZnO films. (iii) STEM images (top) and maps (bottom) of the Raman peak intensity ratio of product/reactant (I_{1442}/I_{1080}) corresponding to disordered and ordered 4-NTP phases. The maps are achieved from *in-situ* TERS spectra measured at different locations on the Au(111) surface during photo-induced 4-NTP dimerization. (C)(i) SERS for reaction pathway investigations. (ii) *In-situ* SERS spectra (bottom) and time-resolved intensity map (top) from individual plasmon-excited Ag NPs in CO_2-saturated water. The peaks in the 750-1800 cm^{-1} region affirm the formation of multi-carbon products. (iii) Bar plot showing the number of detection events across the spectra set for each surface C_1, C_2, C_3, and C_4 species with their percentages. Reprinted and adapted with permission from (A) ref. 65 (B) ref. 61, 64 and (C) ref. 65. Copyright 2021 Dinumol Devasia, Andrew J. Wilson, Jaeyoung Heo, Varun Mohan & Prashant K. Jain. Copyright 2021 Daniel Glass, Raul Quesada-Cabrera, Steven Bardey, Premrudee Promdet, Riccardo Sapienza, Valérie Keller, Stefan A. Maier, Valérie Caps, Ivan P. Parkin, & Emiliano Cortés. Published by American Chemical Society. Copyright 2021 American Chemical Society.

The use of *in-situ/operando* SERS has uncovered key structure-(photocatalytic)activity correlations, including the influence of the photocatalyst's crystal structure (e.g., its exposed crystal phases and crystal defects), as well as the molecular ordering of adsorbates on the crystal surface (Figure 2B-i).[60-62, 64] This is often facilitated by the strategic use of molecules with large Raman cross-sections as probes to study different surfaces, whereby photoinduced changes in their molecular structures, charge distributions and vibronic states can be facilely tracked by monitoring their spectral changes.[60, 61, 63] For instance, experimental observations of surface defects such as oxygen vacancies (V_o) are highly challenging due to their inherent low concentrations and high reactivities, especially at ambient pressures. In one study, a SERS variant – photoinduced enhanced Raman spectroscopy (PIERS) – was employed to probe V_o dynamics on ZnO films by tracking the peak intensity changes of 4-mercaptobenzoic acid

(MBA) with UV exposure, whereby V_o formation increases the MBA band signals via resonant charge transfer while V_o removal reduces the MBA band signals.[61] By loading Au NPs pre-functionalized with MBA on the ZnO films, the PIERS spectra revealed for the first time that the lifetime of *in-situ* generated oxygen vacancies (i.e., longer V_o healing) is more significant in increasing photocatalytic activities than their concentrations (Figure 2B-ii). Besides surface defects, the correlation of adsorbate arrangements with photocatalytic efficiency is also elucidated using *in-situ/operando* SERS. For instance, high-resolution TERS images of the photocatalytic dimerization of 4-nitrothiophenol (4-NTP) molecules over Au(111) surfaces highlight that a disordered 4-NTP adlayer exhibits higher reactivity, with ~82 % product formation surface coverage, compared to ~18% for its well-ordered counterpart (Figure 2B-iii).[64] Briefly, this is achieved by monitoring the peak intensity ratio of the 1442 cm^{-1} product peak to the 1080 cm^{-1} 4-NTP reactant peak. These representative case studies highlight how *in-situ/operando* SERS provides invaluable experimental insights on surface structural and molecular characterizations in photocatalytic systems, which are crucial to develop and optimize better photocatalysts. Although current studies predominantly focus on proof-of-concept model reactions, our aspiration is for these case studies to inspire readers to broaden the application of *in-situ/operando* SERS towards other practical and high-value photocatalytic reactions.

In addition to uncovering fundamental structure-activity correlations, *in-situ/operando* SERS has also revealed critical mechanistic information on the reaction pathways, in terms of identifying the key intermediates, products, and reaction kinetics (Figure 2C-i).[66, 91-94] Several industrially important photocatalytic reactions that have been studied include silane oxidation

to silanol, C-H arylation, and CO_2 reduction (CO_2RR). For instance, *in-situ* SHINERS on CuO-decorated SHINs reveals that the photooxidation of dimethyl(4-(methylthio)phenyl)silane (4-DMPSE) on CuO photocatalysts proceeds *via* an *OH intermediate species in the presence of H_2O_2 oxidant. This is evidenced by the emergence of 708 cm^{-1} peak that was attributed to surface-adsorbed *OH species.[53] Notably, this spectroscopically obtained mechanistic insight was crucial to guide and rationalize the solvent optimization for practical, industrial-scale catalysis using CuO powder instead of CuO NPs by selecting solvents that promote H_2O_2-to-*OH conversion. In another study, *in-situ* SERS (750-1800 cm^{-1} region) on 96 individual Ag NPs during photo-driven CO_2 reduction reactions offered nanoscale and subsecond spatiotemporal resolution to provide a comprehensive profile of the full panel of surface adsorbates and intermediates (Figure 2C-ii).[65] Notably, the study identified several surface species, encompassing a diverse range of C_1-C_4 species such as ethylene glycol, oxalic acid, propanol, and butanol (Figure 2C-iii). These species were previously not elucidated in bulk-level studies because they do not necessarily survive or culminate into the bulk product profile. Such surface chemical knowledge made accessible by *in-situ* nanoscale SERS probing is postulated to better inform computational modeling and engineering of Ag NP catalysts to promote specific reaction pathways for higher selectivity.

In overall, *in-situ/operando* SERS has demonstrated immense potential to advance our mechanistic understanding of photocatalytic reactions. In addition, we would like to highlight the use of *in-situ/operando* SERS to elucidate the roles and behaviors of hot electron carriers in the rapidly emerging domain of plasmon-driven photocatalytic systems, which has been extensively discussed in Warkentin *et al.'s* review.[95]

In-situ/*operando* SERS in solar cells

Solar cells play an indispensable role in advancing clean, renewable, and safe energy systems by harnessing sunlight to generate electricity for diverse sectors, such as residential, commercial, transportation, and agriculture.[96, 97] Similar to photocatalytic systems, the most common approach for *in-situ/operando* SERS studies of solar cells is to deposit the photocatalysts onto support substrates and illuminate the as-prepared platforms with a light source to simulate solar irradiation and an additional laser for SERS excitation. In addition, to probe solar cells in the presence of electric fields or under high pressure, customized photo-Raman cells as described in '*In-situ/operando* SERS in electrocatalytic systems' subsection, or diamond anvil cells equipped with a small hole for sample loading are employed, respectively (Figure 3A). In terms of platform configurations, plasmonic metallic nanostructures and SHINs are usually used, either by direct dropcast on the surface of interest for solid-phase studies or by mixing with target NPs such as semiconductor TiO_2 NPs for liquid-phase measurements.

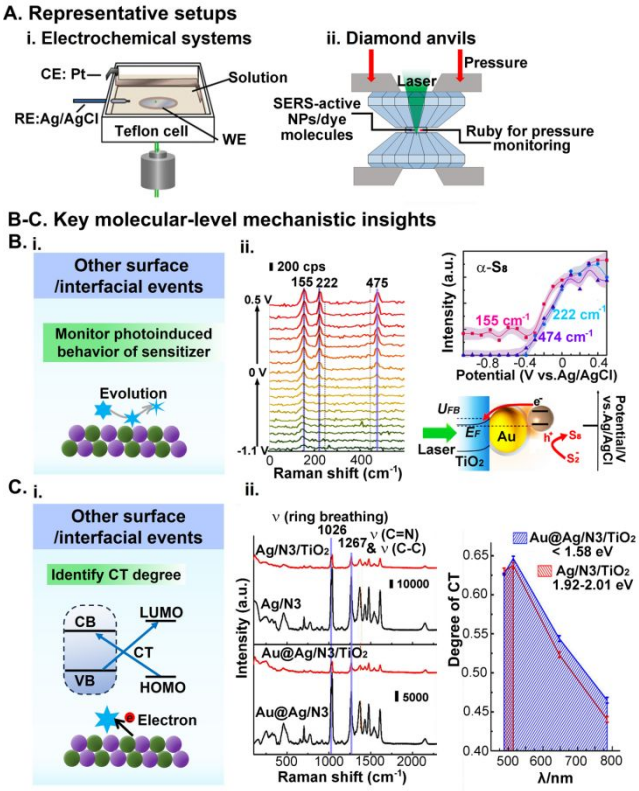

Figure 3. *In-situ*/*operando* SERS in solar cells. (A) Schematics of representative *in-situ/operando* SERS setups in solar cells, including (i) spectroelectrochemical cells and (ii) diamond anvil cells for electrified and pressurized systems, respectively. (B) (i) SERS to monitor photoinduced behaviors of sensitizer molecules. (ii) *In-situ* SERS spectra of PbS QDs/TiO_2/Au/TiO_2 electrode for potentials ranging over −1.1 to 0.5 V (*vs* Ag/AgCl) in an aqueous 0.05 M Na_2S/ 0.1 M NaOH electrolyte. The right upper panel shows potential-dependent Raman intensities of the main peaks. The right lower panel shows the schematic of interfacial hole transfer from PbS QD to a sulfide donor in the electrolyte to produce α-S8. (C) (i) SERS to study charge transfer processes. (ii) *In-situ* SERS spectra of N3 in Ag/N3/TiO_2, Ag/N3, Ag@Au/N3/TiO_2, and Ag@Au/N3 systems (left panel). The two marked peaks at 1026 and 1267 cm^{-1} are using for calculation of the $\boldsymbol{\rho}_{CT}$. The right panel shows the excitation wavelength dependent $\boldsymbol{\rho}_{CT}$ for Ag/N3/TiO_2 and Au@Ag/N3/TiO_2. Reprinted and adapted with permission from (A) ref. 98 (B) ref. 98, and (C) ref. 83. Copyright 2018 and 2019 American Chemical Society.

State-of-the-art solar cell research is strongly motivated by two goals: 1) improve the photoelectric conversion efficiency (PCE) to approach the upper Shockley-Queisser theoretical limit, and 2) overcome the longstanding challenge of poor long-term stability.[58, 82, 83, 98] In this aspect, *in-situ/operando* SERS has demonstrated immense potential to examine different key

surface/interfacial events in solar cells such as photoinduced behaviors of sensitizers (Figure 3B-i). For instance, *in-situ* SERS investigations revealed that increased photocurrents in a PbS quantum dot (QD)-sensitized TiO_2/Au/TiO_2 solar cell with more positive potentials stems from interfacial hole transfer from photoexcited PbS QDs to inorganic sulfide redox couples (S^{2-}/S) electrolytes, which leads to efficient electron-hole separation.[98] Briefly, the SERS spectra indicate that interfacial hole transfer occurs *via* the formation of cyclo-octasulfur (α-S_8), as evidenced by characteristic peak emergences at 155, 222, and 474 cm^{-1} (Figure 3B-ii). In another study, *in-situ* SHINERS of a mixture of TiO_2 and ruthenium-based N719 dye molecules reveals that N719 undergoes photoinduced decarboxylation, which can potentially be one of the primary reasons that cause poor N719 sensitization and long-term operational inefficiency in dye-sensitized solar cells (DSSCs).[58] The photoinduced decarboxylation is evidenced by the observed band splitting of 1545 cm^{-1} C=C stretching mode, and respective blue- and redshifts of 1478 cm^{-1} C=N stretching and 1612 cm^{-1} C=C stretching modes, which are well-aligned with simulated spectral changes of N719 and decarboxylated N719. These case studies thus highlight how *in-situ/operando* SERS can provide potentially in-depth understanding of the sensitizer photoactivity on different semiconductor surfaces to guide the rational design of solar cells with increased photovoltaic performances.

In addition, *in-situ*/*operando* SERS is intrinsically well-suited to study charge carrier dynamics at the donor-acceptor interface, including charge generation, separation, recombination, and transfer, since CT is involved in one of the two key SERS enhancement mechanisms (Figure 3C-i).[83-85, 99] For instance, the use of *in-situ/operando* SERS has unveiled fundamental interfacial information on how the integration of bimetallic Au@Ag NPs reduce

the CT threshold of N3 dye-based DSSCs, which is essential to expand the CT response range and enhance CT efficiency in the low-energy region.[84] Using the peak intensity ratio of N3's 1267 cm^{-1} CT-dependent peak against its 1026 cm^{-1} CT-independent peak at different laser wavelengths to estimate CT probability (ρ_{CT}), it was determined that the CT threshold is reduced from 2.47 eV in Ag/N3/TiO_2 system to < 1.58 eV in bimetallic Au@Ag/N3/TiO_2 system (Figure 3C-ii). The decreased CT threshold is proposed to arise from energy level equilibration and Ag activation at the core-shell interface, which lowers the energy levels. In another study, *in-situ* SERS is used to investigate the effect of external stimuli such as pressure on the interfacial CT processes of TiO_2@N719 and TiO_2@N719@Ag.[83] Briefly, the CT probability ρ_{CT}, which is positively correlated with the peak intensity ratio of N719's 1266 cm^{-1} CT-dependent peak against its 1024 cm^{-1} CT-independent ring breathing peak, is favored with increasing external pressures up to 2.48 and 1.37 GPa, respectively. The *in-situ* spectral results thus affirm that high external pressures effectively tune the TiO_2 bandgaps to increase ρ_{CT}.[83]

From a broader perspective, these case studies collectively highlight the utility of *in-situ/operando* SERS as a facile approach to obtaining mechanistic information on surface/interfacial events on diverse surfaces, including single-crystal, polycrystalline, and amorphous surfaces. Although current SERS investigations of solar cells and solar cell-like systems predominantly focus on DSSCs and QDSSCs, we anticipate the growing adoption of similar methodologies for other emerging solar cell technologies such as perovskite solar cells.

In-situ/*operando* SERS in electrocatalytic systems

The conversion of electrical energy to chemical fuels including H_2, NH_3, formic acid, formate, carbon monoxide, and various multicarbon C_{2+} products hold immense appeal due to their high energy densities.[67-69, 71, 100-103] Typically, the *in-situ/operando* SERS studies of electrocatalytic systems are performed in customized spectroelectrochemical cells, with the working electrode illuminated from above while the counter and reference electrodes are positioned away from the laser beam path (Figure 4A). Various electrochemical techniques including cyclic voltammetry, chronoamperometry, and electrochemical impedance spectroscopy can be integrated with SERS by linking the spectroelectrochemical cell to a Raman spectrometer and an electrochemical workstation. For the SERS-active working electrode, it can be directly prepared *via* surface roughening or dropcast assembly of plasmonic nano-electrocatalysts on the electrode surface. Non-plasmonic electrocatalysts can be modified with SHINs or hybridized with plasmonic nanostructures in plasmonic core-electrocatalytic satellite configurations to facilitate *in-situ/operando* SERS studies.[67]

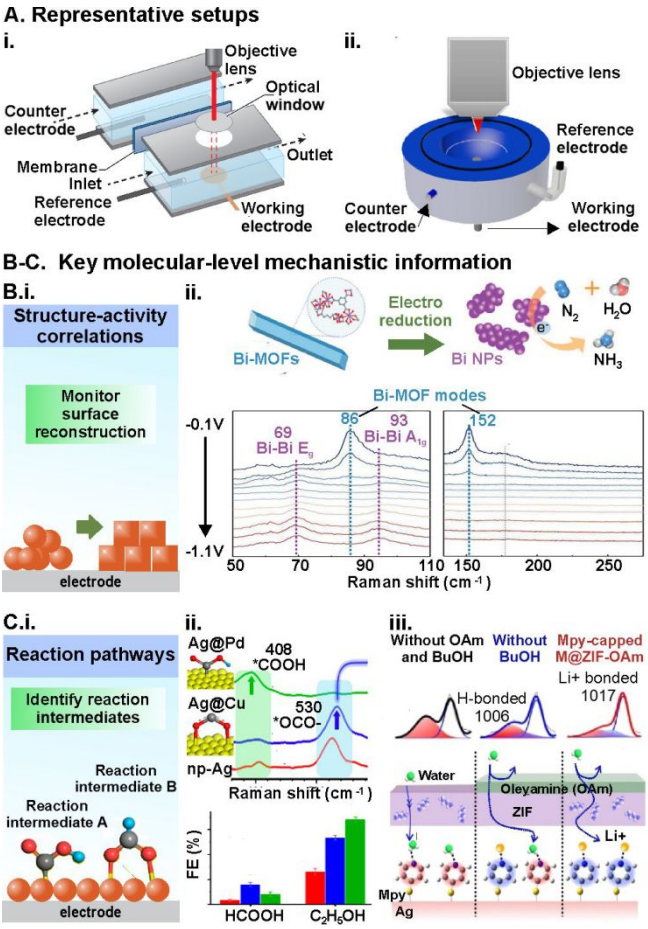

Figure 4. Applications of SERS in electrocatalytic systems. (A) Schematics of representative *in-situ/operando* setups. (B) (i) SERS to monitor surface reconstruction dynamics. (ii) *In-situ* spectra of the Bi-MOF catalyst immersed into a thin electrolyte film from −0.1 to −1.1 V_{RHE}. The schematic for *in-situ* electroreduction-derived transformation from nanorods to nanoparticles included as top inset. (C) (i) SERS to identify key reaction intermediates for reaction pathway monitoring. (ii) *In-situ* SERS spectra on three electrodes during CO_2RR, with schematics of intermediates included (top), and corresponding faradaic efficiencies of different products. (iii) Schematic depicting the diffusion of water into MPY-capped M@ZIF and M@ZIF-OAm platforms, with respective deconvoluted bands on the breathing modes after water addition. Reprinted and adapted with permission from (A) refs. 101 and 102, (B) ref. 70, and (C) refs. 72, 73. Copyright 2021, Proceedings of the National Academy of Sciences. Copyright 2023 Bjorn Hasa, Yaran Zhao, and Feng Jiao. Copyright 2020 American Chemical Society. Copyright 2020 WILEY-VCH Verlag GmbH & Co. KGaA, Weinheim.

Key electrocatalytic reactions that have been probed with *in-situ/operando* SERS include hydrogen evolution reaction (HER), oxygen evolution reaction (OER), CO_2 reduction reaction (CO_2RR), as well as N_2 and NO_3^- reduction (NRR and NO_3RR). In terms of structure-activity

correlations, *in-situ/operando* SERS offers crucial molecular-level insights into the surface reconstruction dynamics and true active sites of electrocatalysts (Figure 4B-i). Such information is intimately linked to the observed faradaic efficiencies and product selectivity of different electrocatalysis reactions.[67-69, 71] For instance, *in-situ* SERS monitoring of NRR on nanorod-like Bi-based metal organic frameworks (MOFs) affirms the importance of the electrocatalysts' *in-situ* structural rearrangement into zero-valent Bi NPs to afford significant NH_3 yield of 3.25 ± 0.08 μg cm^{-2} h^{-1} at −0.7 V_{RHE} and a faradaic efficiency of 12.11 ± 0.84% at −0.6 V_{RHE}.[70] The *in-situ* structural rearrangement is revealed by peak disappearances at 86 and 152 cm^{-1}, indexed to Bi-MOF bonding, and concomitant peak emergences at 69 and 93 cm^{-1}, corresponding to E_g and A_{1g} stretching modes of Bi-Bi bonds, at negative applied potentials (Figure 4B-ii).

As for studying electrocatalytic reaction pathways, *in-situ/operando* SERS has revealed key reaction intermediates, which are essential to deduce the selectivity mechanisms for complex reactions involving multiple electron and proton transfer steps since there are many potential reaction routes (Figure 4C-i). For intermediates with distinct Raman fingerprints, the evolution of their characteristic vibrational modes can be directly tracked using SERS. For example, *in-situ* SERS was used to understand the selective CO_2RR to HCOOH and C_2H_5OH on electrocatalytic nanoporous Ag electrodes modified with Cu (np-Ag@Cu) and Pd (np-Ag@Pd), respectively.[72] For np-Ag@Pd, CO_2 adsorbs *via* *COOH intermediate with a top-site adsorption structure to selectively produce C_2H_5OH, recording more intense *COOH out-of-plane wagging mode at 408 cm^{-1}(Figure 4C-ii). For np-Ag@Cu, CO_2 preferentially adsorbs *via*

* OCO^- instead with a bridge-site adsorption structure to selectively yield HCOOH, as evidenced by the more intense *COOH out-of-plane wagging mode at 530 cm^{-1}.

On the other hand, intermediates with intrinsically weak Raman signals can be indirectly monitored with probe molecules. For instance, *in-situ* SERS was employed to affirm that their hybrid zeolitic-imidazolate framework-based electrocatalyst effectively suppresses water adsorption on the electrocatalytic surface for preferential NRR over HER (Figure 4C-iii).[73] Since water is a poor Raman scatterer, the detection of adsorbed water is achieved using 4-mercaptopyridine (MPY) as a probe. The observed small increase in the relative intensities of the 1006 cm^{-1} hydrogen-bonded to 1017 cm^{-1} Li^+-bonded MPY ring breathing modes over 2 h indicates that the initial MPY-Li^+ interactions are not replaced with water, thus affirming that few water molecules can access the electrocatalyst. Collectively, these examples highlight how key intermediates (or the lack thereof) at the electrocatalyst-electrolyte interface can be univocally identified and verified using *in-situ/operando* SERS to elucidate the mechanistic pathways, regardless of their inherent Raman scattering nature.

Besides probing on-surface dynamics, *in-situ/operando* SERS is also indispensable to track other interfacial events, which complements acquired surface-associated information and enables researchers to obtain a holistic view of the complete electrocatalytic reaction mechanism. For instance, one essential yet poorly understood aspect of electrocatalytic systems is the role of the electrolyte, including the individual effects of the electrolyte pH, ionic species present, and the solvent type. In one study, *in-situ* SHINERS was leveraged to investigate how the inclusion of co-catalyst interfacial cations improves HER rates on atomically flat Pd single crystal surfaces, using the strong signal enhancement at the junctions between SHINs and Pd

substrate.[54] The authors determine that an increase in the electrolyte $NaClO_4$ concentration enhances HER due to an increase in $Na{\cdot}H_2O$ proportion which enables a more structured ordering of interfacial water for better charge transfer efficiency. This is affirmed using SHINERS by comparing the intensity ratios of the O-H stretching modes of Na^+ ion-hydrated interfacial water ($Na{\cdot}H_2O$, indexed at ~3540 cm^{-1}) and hydrogen-bonded interfacial water ($HB{\cdot}H_2O$, indexed at ~3155 and 3350 cm^{-1}).

Overall, these representative examples highlight the significant progress achieved to date in deciphering the full roadmap of various key electrocatalytic reactions using *in-situ/operando* SERS. This in-depth mechanistic understanding is critical to guide the design of next-generation electrocatalysts with improved Faradaic efficiencies and higher product selectivity.

In-situ/*operando* SERS in fuel cells

To date, there are diverse fuel cell technologies that cater to different applications ranging from electric vehicles to power plants and stations, typically categorized by their electrolyte type and fuel source.[104] The setups for *in-situ/operando* SERS studies of these diverse fuel cell systems can be tailored to match the individual operating conditions. For example, SERS investigations of fuel cells with liquid electrolytes, such as proton-exchange membrane and alkaline anion exchange fuel cells (PEMFCs, AEMFCs), can be performed in standard three-electrode electrochemical setups (Figure 5A-i). On the other hand, fuel cells of high operating temperatures, such as solid oxide fuel cells (SOFCs; operate at 600 – 1000 ^oC) require high-temperature chambers to simulate the actual operating conditions (Figure 5A-ii). The SERS-active electrode can be prepared *via* similar methodologies as other electrocatalytic systems,

either through direct dropcast of plasmonic nanoelectrocatalysts on the electrode surface or modification with bifunctional core@shell, core-satellites, SHINs, or SHIN-satellites nanostructures. In particular, SHINs are favored to probe high-temperature fuel cell systems due to the additional thermal stability bestowed by their protective dielectric shell.

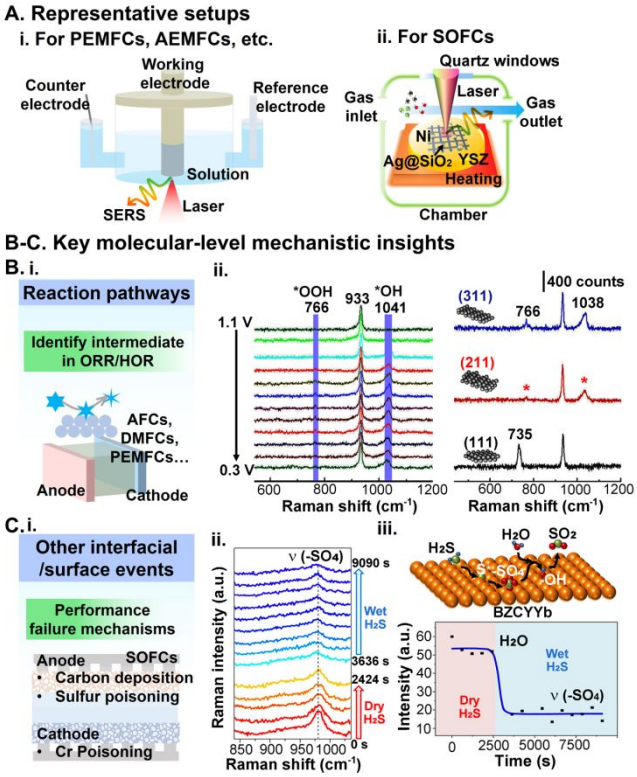

Figure 5. *In-situ/operando* SERS applied in fuel cells. (A) Schematic of representative *in-situ/operando* SERS setups for fuel cells, namely (i) three-electrode electrochemical system and (ii) high-temperature chambers. (B) (i) SERS to elucidate ORR/HOR reaction pathways. (ii) In-situ SHINERS spectra on Pt(211) surface under different potentials (left) and on different Pt(*hkl*) surfaces at 0.8 V (right) in 0.1 M O_2-saturated $HClO_4$ solution. (C) (i) SERS to elucidate key surface/interfacial events including catalyst degradation and poisoning. (ii) *In-situ* SERS spectra of a Ni−BZCYYb electrode when the fuel was changed from dry to wet 100 ppm H_2S/H_2 at 500 °C. (iii) Evolution of the -SO_4 peak intensity before ande after H_2O vapor injection (lower). Proposed mechanism of water-mediated sulfur tolerance *via* H_2S-to-SO_2 conversion (upper). Reprinted and adapted with permission from (A) ref. 107 (B) ref. 55, and (C) ref. 80. Copyright 2020, 2021 American Chemical Society.

A key application of *in-situ*/*operando* SERS in fuel cells is to investigate the reaction

pathways of major half-cell reactions including hydrogen oxidation reaction (HOR) and oxygen reduction reaction (ORR) on different catalytic surfaces, which strongly govern their reaction dynamics and determine the resultant activity and/or stability (Figure 5B-i).[15, 55, 57, 74-78, 105] For instance, *in-situ* SHINERS is proven instrumental in clarifying the ORR pathways on high-index Pt(211) and Pt(311) surfaces in acidic conditions through direct observations of both *OH and *OOH intermediates at 1040 and 765 cm^{-1}, respectively.[55] Notably, the higher intensity of the 765 cm^{-1} band for Pt(311) indicates that *OOH binds more strongly to Pt(311) than Pt(211) surfaces, which accounts for its reduced ORR activity (Figure 5B-ii). Leveraging the SHINERS strategy, the ORR mechanism was also elucidated on low-index Pt(*hkl)* surfaces, and on Pt(*hkl*) surfaces in nonaqueous electrolytes.[56, 57] It is worth noting that the ORR reaction pathway over Pt catalyst has remained controversial for a long time, despite Pt-based catalysts being highly popular candidates for ORR catalysis. These fundamental mechanistic insights would thus provide useful theoretical guidance for the rational design of high-activity ORR catalysts.

In-situ SERS is also valuable for obtaining direct spectroscopic evidence to establish structure-activity correlations, such as the effect of metal doping on the activity and stability of catalysts.[15, 74, 105] In one study, the *in-situ* SERS spectra show that Ni doping in Pt-based catalysts decreases the *OH-O binding energy in $*HO_2$ intermediate to achieve more efficient electron transfer for improved ORR performance, as evidenced by the observed redshift of $*HO_2$'s vibrational mode.[15] The observed redshift can be explained by the higher orbital overlap which enhances the binding and back-donation between the p orbital of O(H) and d orbital of Pt on the PtNi surface, thus decreasing the *OH-O binding energy and redshifting the associated $*HO_2$ vibrational mode. Related studies also unveil that incorporating CoSn and Pd instead of

Ni can also improve ORR by optimizing HO_2 adsorption configuration and lowering the *HO-O binding energy *via* the strain and electronic effects respectively. [61-63] Collectively, these representative case studies highlight how *in-situ/operando* SERS monitoring of intermediate evolution is essential to better rationalize the observed catalyst performances and guide strategic catalyst design, screening, and optimization for fuel cell systems.

Another key area of high research value in the field of fuel cells is to investigate various catalyst failure mechanisms at the electrode-electrolyte interface, such as catalyst degradation and catalyst poisoning by air contaminants including SO_x, NO_x, and organic impurities (Figure 5C-i). The obtained *in-situ/operando* mechanistic insights are critical to guide the strategic design of mitigation strategies for more durable fuel cell systems, which is one of the bottleneck problems hindering the commercial application of many emerging fuel cell technologies.[79-81, 106, 107] For instance, in one study, *in-situ* SERS studies of the conversion of highly toxic H_2S reveals that the presence of water enhances sulfur tolerance of Ni-$BaZr_{0.1}Ce_{0.7}Y_{0.1}Yb_{0.1}O_{3-\delta}$ (BZCYYb) anodes in SOFCs.[80] With exposure to water vapor, H_2S which is adsorbed on the BZCYYb anode as $–SO_4$ (peak at 980 cm^{-1}), is effectively removed by the following reaction: $H_2O + SO_4^{2-} + 2e^- \rightarrow 4OH^- + SO_2$ to enhance sulfur tolerance, as evidenced by the rapid disappearance of the 980 cm^{-1} peak (Figures 5C-ii, 5C-iii). In another study, *operando* SERS reveals the Cr poisoning mechanism on thin-film $La_{0.6}Sr_{0.4}Co_{0.2}Fe_{0.8}O_3$ (LSCF) cathode (deposited on Gd-doped ceria substrate, GDC), which allows the authors to develop more Cr-tolerant LSCF cathodes.[106] The results show that when the LSCF is in direct contact with the Cr alloy, Cr is converted to insulating $SrCrO_4$ which blocks the active ORR sites, as evidenced by the observation of multiple bands between 800 and 900 cm^{-1}. Leveraging these insights, the

authors coated the LSCF cathodes with ORR-active but Cr-inert catalysts, namely $PrNi_{0.5}Mn_{0.5}O_3$ and PrO_x, and additional SERS analyses affirm that the hybrid LSCFs exhibit excellent Cr tolerance, with no $SrCrO_4$ peaks while maintaining high ORR activity.

In all, *in-situ/operando* SERS thus establishes itself as an invaluable tool to directly and sensitively probe different key aspects of fuel cells, ranging from catalytic reaction pathways to performance failure. These comprehensive mechanistic revelations are crucial in designing more durable and efficient fuel cells for more sustainable and reliable power generation.

In-situ/*operando* SERS in batteries

Battery systems represent one of the most mature energy systems in which *in-situ/operando* SERS has been utilized, owing to the urgent technological need to accommodate modern energy requirements such as electric vehicles.[88, 108-113] To enable *in-situ* SERS measurements, the electrodes and separator are typically sealed in an electrolyte-filled Raman cell of various tailored configurations such as coin cells, with a quartz window for effective laser beam exposure and Raman signal acquisition (Figure 6A-i). Due to the high reactivity of lithium metal, which is the most studied anode material in batteries, the electrochemical cell usually needs to be airtight to prevent air and moisture exposure. However, one interesting setup that has been reported specifically for combinatorial screening involves using a pipette probe containing electrolyte solution and a quasi-reference counter electrode (QRCE) over a Si electrode, with SHINs assembled atop the Si electrode (Figure 6A-ii).[59, 89, 90] Regardless of the platform configuration, the spectroelectrochemical cell is then connected to both a Raman spectrometer and an electrochemical workstation, similar to other electrocatalytic systems. As

for the SERS-active substrates, SERS-active working electrodes such as Au, Ag and Cu are commonly electrochemically roughened to achieve varied roughness from submicron to nanoscale using different voltage waveforms, cycle numbers and potential windows. To achieve more precise control and more intense SERS enhancement, designer SERS-active nanostructures and SHINs can be deposited on the working electrode instead, which is important to effectively elucidate the compositions and dynamics within the battery systems because the target interfacial species and reaction intermediates are usually low in concentrations.

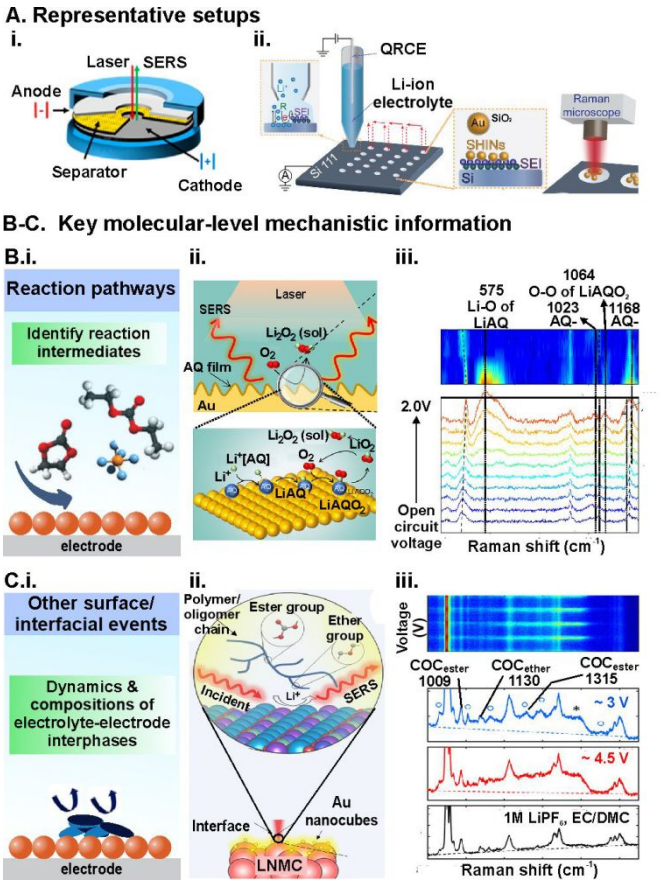

Figure 6. Application of SERS in batteries. (A) Schematics of (i) coin cell setup and (ii) combinatorial electrochemical screening of SEI formation using SHINERs. (B) (i) SERS to identify redox intermediates and products. (ii) Schematic of *in-situ* SERS study of AQ-catalyzed solution-mediated ORR on a model Au-AQ electrode. The rough Au surface represents the enhanced Raman substrate. (iii) *In-situ* SERS (bottom) and corresponding Raman intensity as a function of the potential on an Au-AQ electrode in 0.1 M O_2-saturated $LiClO_4$–

CH_3CN. The characteristic peaks indexed to the intermediates are indicated. (C) (i) SERS to unravel interfacial events at electrode-electrolyte interphases. (ii) Schematic of oligomerization mechanism during CEI formation. Solvent molecules (EC and DMC) polymerize with ether and ester linkages and adsorb on the LNMC surface. (iii) *Operando* Raman spectral evolution acquired in four consecutive cycles for an LNMC electrode (top). The cell was cycled between 3–4.5 V and each spectrum is acquired within a voltage interval of 50 mV. Representative spectra were acquired at the low voltage state (~3 V, blue) and the high voltage state (~4.5 V, red) in comparison with a Raman spectrum of a 1 M EC/DMC $LiPF_6$ electrolyte (black) (bottom). Raman bands related to CEI are marked with blue circles and the band likely contributed by oxidation of the electrolyte is marked with an asterisk. Reprinted and adapted with permission from (A) refs. 59 and 89, (B) ref. 86, and (C) ref. 88. Copyright 2019, 2021 American Chemical Society. Copyright 2022 Daniel Martín-Yerga, David C. Milan, Xiangdong Xu, Julia Fernández-Vidal, Laura Whalley, Alexander J. Cowan, Laurence J. Hardwick, Patrick R. Unwin. Angewandte Chemie International Edition published by Wiley-VCH GmbH.

For battery systems, *in-situ/operando* SERS has provided numerous spectroscopic evidence for an in-depth understanding of the redox reaction pathways at the electrode materials, including the charge and discharge products, as well as reactive, short-lived intermediates (Figure 6B-i).[59, 86, 87, 89, 90] These redox chemistries can be highly complex due to multi-electron processes and multi-phase transitions, such as in the case of lithium-sulfur batteries involving sulfur and lithium polysulfides. For instance, soluble catalysts such as reduction mediators have been successfully employed in solution-mediated oxygen reduction reaction (ORR) to regulate cathode passivation from discharge product Li_2O_2, particularly in Li-O_2 batteries (i.e., the 'sudden-death' phenomenon). However, the exact reaction pathway remains controversial to date due to a lack of direct *in situ* evidence. In this aspect, a recent study leveraged *in-situ* SERS to obtain direct spectroscopic evidence of the reaction intermediates and related elementary steps in aprotic Li-O_2 batteries to clarify the mechanism at the molecular level (Figure 6B-ii).[86] The investigation utilized an anthraquinone (AQ)-immobilized Au electrode/CH_3CN model

interface to represent the complex battery system, in which AQ is the reduction mediator. Briefly, the authors found that AQ first interacts with Li^+ to form Li^+[AQ], which is then preferentially reduced and combined with O_2 to form $LiAQO_2$ intermediates, as evidenced by the shift of AQ's A_g mode from 481 cm^{-1} to 488 cm^{-1} and subsequent band emergence of O–O stretch mode at 1064 cm^{-1} (Figure 6B-iii). The $LiAQO_2$ finally releases LiO_2 to form Li_2O_2 *via* disproportionation in the bulk electrolyte.

In addition to deciphering the electrode's redox chemistries, *in-situ/operando* SERS has also made significant strides in fundamental studies of the compositions and dynamics of electrolyte interphases during charge and discharge cycles/states (Figure 6C-i). These surface/interfacial events are highly challenging to investigate due to the heterogeneous and complex distributions of the electrolyte interphases and potential electrolyte interferences. In one study, *operando* SERS was employed to unravel the correlations between the cathode-electrolyte interphase (CEI) dynamics and state-of-charge (SOC) of $LiNi_{0.33}Co_{0.33}Mn_{0.33}O_2$ (LNMC) cathode in a Li-ion battery, with ethylene carbonate/dimethyl carbonate/$LiPF_6$ as electrolyte (Figure 6C-ii).[88] By depositing Au nanocubes on the LMNC, the authors observed the emergence of vibrational modes associated with ester and ether linkages in the 850 – 1900 cm^{-1} region (ν_{Mid}) such as ν(C-O-C) stretching, ν(C=O) stretching, and δ(C-H) bending, which indicated that the ester molecules oligomerize during CEI formation (Figure 6C-iii). They further uncover the polymerization dynamics as a function of cell potential, whereby polymerization is more favored at lower voltages (i.e., in the discharged state or lower SOC), with maximal CEI-associated band intensities. In another example, the authors used *in-situ* SHINERS with SHINs-decorated tin anodes to track the solid-electrolyte interphase (SEI)

formation in a coin cell-like *operando* Raman cell filled with ethylene carbonate/diethyl carbonate (EC-DEC)/$LiPF_6$ electrolyte.[59] By observing the peak emergences at 501-513, 1074 and 1266 cm^{-1}, *in-situ* SERS studies reveal that the EC-DEC electrolyte mixture is predominantly reduced to diethyl 2,5-dioxahexane dicarboxylate (DEDOHC) and lithium ethylene monocarbonate (LEMC) on tin electrodes. The observed products are in stark contrast with other often-reported electrolyte reduction products on Au and Ni electrodes such as lithium ethylene decarbonate, LiF and Li_2CO_3. Notably, the cyclic formation of electrolyte-soluble DEDOHC accounts for the poor passivating properties of tin in EC-DEC $LiPF_6$ electrolyte and for its large irreversible capacity, thus offering crucial insights into the degradation of organic electrolytes and tin-specific interfacial instability. By obtaining accurate descriptions of the compositions of electrolyte interphases and their voltage-dependent evolutions, researchers can thus more effectively design new electrolyte and electrode formulations for optimized battery operation.

Collectively, these case studies highlight the importance of *in-situ/operando* SERS to better elucidate the mechanistic origins behind battery performance by clarifying reaction pathways and surface/interfacial events that are previously elusive or inconclusive.

Conclusion and outlook

By offering molecule-specific spectral fingerprints with ultrahigh sensitivity, nanoscale spatial resolution, and subsecond time resolution, *in-situ*/*operando* SERS has thus established itself as a powerful and indispensable technique to advance energy research. To further tap on the potential that *in-situ/operando* SERS offers, we identify several challenges and potential

research directions.

One challenge to overcome is to precisely isolate the target SERS signals from species of interest in complex, real-life energy systems comprising multiple components, reaction pathways, and interfacial events, which often result in highly complicated and overlapping spectra. Moreover, this is exacerbated by the low Raman cross-sections of certain target species such as adsorbed oxygen and hydrogen, whose weak signals may be easily masked by interfering signals from other species present in the energy system. To tackle this challenge, we have seen the burgeoning use of advanced data analysis techniques, such as multivariate analysis and machine learning algorithms, to facilitate the extraction and identification of specific SERS signals from complex backgrounds.[114, 115]

A second challenge is to further improve the temporal resolution of SERS to better capture spectroscopic evidence of transient, short-lived events that occur on femto- to picosecond timescales. In this aspect, the strategic use of ultrafast SERS, which combines SERS with ultrafast spectroscopy using ultrafast pump pulses, is a highly promising SERS variant to watch these molecular and molecule-substrate dynamics on their inherent timescales.[116] Although the specific use of ultrafast SERS in the energy systems of interest in this mini-review is still in its infancy stages, we anticipate a rapid increase in its application for energy-related investigations. It is also of note that ultrafast SERS is compatible with key SERS-active platform configurations described in the earlier sections, and thus we postulate that it can be readily adopted to study energy systems.

Next, to advance these energy systems toward practical, real-life applications, it is also important to apply these *in-situ*/*operando* techniques to more industrially relevant setup

configurations, which may exhibit different reaction dynamics and kinetics, such as transiting from conventional three-electrode systems to gas-diffusion electrodes in electrocatalytic systems. It will also be highly advantageous to develop techniques that are compatible with plasmonics in the near-to-far UV range to further broaden the substrate scope. On this note, we would like to highlight several promising developments in enhancing SERS capabilities for energy research. Notable developments include the combination of SHINERS with scanning electrochemical cell microscopy for high-throughput screening of SEI formation under different electrochemical conditions, and the development of depth-sensitive plasmon-enhanced Raman spectroscopy to overcome the surface-sensitive nature of SERS and characterize SEI at different depths.[89, 90]

Overall, as the requirements of energy systems continue to increase, we believe that new SERS technologies will emerge to overcome the challenges faced by existing SERS techniques and enable better *in-situ/operando* studies of more energy systems such as perovskite solar cells, triboelectric nanogenerators, thermoelectric devices, piezoelectric materials etc. By embracing these opportunities and addressing the existing challenges, we are confident that SERS will continue to be a transformative tool in advancing energy systems.

Acknowledgements

This research is supported by Singapore National Research Foundation Central Gap Fund (NRF2020NRF-CG001-010), Competitive Research Programme (NRF-CRP26-2021-0002), National Research Foundation Investigatorship (NRF-NRFI08-2022-0011), A*STAR AME Individual Research Grant (A20E5c0082) and Institute for Digital Institute for Digital Molecular Analytics and Science (IDMxS). J.R.T.C. acknowledges scholarship support from Nanyang Technological University, Singapore. We would also like to acknowledge the funding supports from Jiangsu Specially-Appointed Professor project (1046010241230830), National Natural Science Foundation of China (22108030) and Natural Science Foundation of Shanghai (22ZR1401500).

References

1. Höök, M.; Tang, X. Depletion of Fossil Fuels and Anthropogenic Climate Change—A Review. *Energy Policy* **2013**, *52*, 797-809.

2. Ahmadi, M. H.; Ghazvini, M.; Alhuyi Nazari, M.; Ahmadi, M. A.; Pourfayaz, F.; Lorenzini, G.; Ming, T. Renewable Energy Harvesting with the Application of Nanotechnology: A Review. *International Journal of Energy Research* **2019**, *43*, 1387-1410.

3. Yao, K. P. C.; Kwabi, D. G.; Quinlan, R. A.; Mansour, A. N.; Grimaud, A.; Lee, Y.-L.; Lu, Y.-C.; Shao-Horn, Y. Thermal Stability of Li_2O_2 and Li_2O for Li-Air Batteries: In Situ XRD and XPS Studies. *Journal of The Electrochemical Society* **2013**, *160*, A824.

4. Liu, X. H.; Liu, Y.; Kushima, A.; Zhang, S.; Zhu, T.; Li, J.; Huang, J. Y. In Situ TEM Experiments of Electrochemical Lithiation and Delithiation of Individual Nanostructures. *Adv. Energy Mater.* **2012**, *2*, 722-741.

5. Endres, F.; Borisenko, N.; El Abedin, S. Z.; Hayes, R.; Atkin, R. The interface ionic liquid(s)/electrode(s): In situSTM and AFM measurements. *Faraday Discussions* **2012**, *154*, 221-233.

6. Wen, R.; Hong, M.; Byon, H. R. In Situ AFM Imaging of Li–O_2 Electrochemical Reaction on Highly Oriented Pyrolytic Graphite with Ether-Based Electrolyte. *Journal of the American Chemical Society* **2013**, *135*, 10870-10876.

7. Mu, C.; Lv, C.; Meng, X.; Sun, J.; Tong, Z.; Huang, K. In Situ Characterization Techniques Applied in Photocatalysis: A Review. *Adv. Mater. Interfaces* **2023**, *10*, 2201842.

8. Hatchard, T. D.; Dahn, J. R. In Situ XRD and Electrochemical Study of the Reaction of Lithium with Amorphous Silicon. *Journal of The Electrochemical Society* **2004**, *151*, A838.

9. Bañares, M. A. Operando Methodology: Combination of in Situ Spectroscopy and Simultaneous Activity Measurements under Catalytic Reaction Conditions. *Catalysis Today* **2005**, *100*, 71-77.

10. Qiao, Y.; Hu, R.; Gu, Y.; Tang, F.-J.; Luo, S.-H.; Zhang, H.-T.; Tian, J.-H.; Cheng, J.; Tian, Z.-Q. Exploring New Generation of Characterization Approaches for Energy Electrochemistry—from Operando to Artificial Intelligence. *Sci. Sin. Chim.* **2024**, 54.

11. Yang, S.; Dai, X.; Stogin, B. B.; Wong, T.-S. Ultrasensitive Surface-Enhanced Raman Scattering Detection in Common Fluids. *Proc. Natl. Acad. Sci. USA* **2016**, *113*, 268-273.

12. Li, J. F.; Huang, Y. F.; Ding, Y.; Yang, Z. L.; Li, S. B.; Zhou, X. S.; Fan, F. R.; Zhang, W.; Zhou, Z. Y.; Wu, D. Y.; Ren, B.; Wang, Z. L.; Tian, Z. Q. Shell-Isolated Nanoparticle-Enhanced Raman Spectroscopy. *Nature* **2010**, *464*, 392-395.

13. Bao, H.; Motobayashi, K.; Ikeda, K. Engineered Au@CuO Nanoparticles for Wide-Range Quantitation of Sulfur Ions by Surface-Enhanced Raman Spectroscopy. *Analytical Chemistry* **2022**, *94*, 17169-17176.

14. Bao, H.; Motobayashi, K.; Zhang, H.; Cai, W.; Ikeda, K. In-situ Surface-Enhanced Raman Spectroscopy Reveals a Mars–van Krevelen-Type Gas Sensing Mechanism in Au@SnO_2 Nanoparticle-Based Chemiresistors. *The Journal of Physical Chemistry Letters* **2023**, *14*, 4113-4118.

15. Ze, H.; Chen, X.; Wang, X.-T.; Wang, Y.-H.; Chen, Q.-Q.; Lin, J.-S.; Zhang, Y.-J.; Zhang, X.-G.; Tian, Z.-Q.; Li, J.-F. Molecular Insight of the Critical Role of Ni in Pt-Based Nanocatalysts for Improving the Oxygen Reduction Reaction Probed Using an In Situ SERS Borrowing Strategy. *Journal of the American Chemical Society* **2021**, *143*, 1318-1322.

16. Zhang, T.; Sun, Y.; Hang, L.; Li, H.; Liu, G.; Zhang, X.; Lyu, X.; Cai, W.; Li, Y. Periodic Porous Alloyed Au–Ag Nanosphere Arrays and Their Highly Sensitive SERS Performance with Good Reproducibility and High Density of Hotspots. *ACS Applied Materials & Interfaces* **2018**, *10*, 9792-9801.

17. Furube, A.; Hashimoto, S. Insight into Plasmonic Hot-Electron Transfer and Plasmon Molecular Drive: New Dimensions in Energy Conversion and Nanofabrication. *NPG Asia Materials* **2017**, *9*, e454-e454.

18. Lan, L.; Gao, Y.; Fan, X.; Li, M.; Hao, Q.; Qiu, T. The Origin of Ultrasensitive SERS Sensing Beyond Plasmonics. *Frontiers of Physics* **2021**, *16*, 43300.

19. Cong, S.; Liu, X.; Jiang, Y.; Zhang, W.; Zhao, Z. Surface Enhanced Raman Scattering Revealed by Interfacial Charge-Transfer Transitions. *The Innovation* **2020**, *1*.

20. Langer, J.; Jimenez de Aberasturi, D.; Aizpurua, J.; Alvarez-Puebla, R. A.; Auguié, B.; Baumberg, J. J.; Bazan, G. C.; Bell, S. E. J.; Boisen, A.; Brolo, A. G.; Choo, J.; Cialla-May, D.; Deckert, V.; Fabris, L.; Faulds, K.; García de Abajo, F. J.; Goodacre, R.; Graham, D.; Haes, A. J.; Haynes, C. L.; Huck, C.; Itoh, T.; Käll, M.; Kneipp, J.; Kotov, N. A.; Kuang, H.; Le Ru, E. C.; Lee, H. K.; Li, J.-F.; Ling, X. Y.; Maier, S. A.; Mayerhöfer, T.; Moskovits, M.; Murakoshi, K.; Nam, J.-M.; Nie, S.; Ozaki, Y.; Pastoriza-Santos, I.; Perez-Juste, J.; Popp, J.; Pucci, A.; Reich, S.; Ren, B.; Schatz, G. C.; Shegai, T.; Schlücker, S.; Tay, L.-L.; Thomas, K. G.; Tian, Z.-Q.; Van Duyne, R. P.; Vo-Dinh, T.; Wang, Y.; Willets, K. A.; Xu, C.; Xu, H.; Xu, Y.; Yamamoto, Y. S.; Zhao, B.; Liz-Marzán, L. M. Present and Future of Surface-Enhanced Raman Scattering. *ACS Nano* **2020**, *14*, 28-117.

21. Sharma, B.; Frontiera, R. R.; Henry, A.-I.; Ringe, E.; Van Duyne, R. P. SERS: Materials, Applications, and the Future. *Materials Today* **2012**, *15*, 16-25.

22. Lu, X.; Huang, Y.; Liu, B.; Zhang, L.; Song, L.; Zhang, J.; Zhang, A.; Chen, T. Light-Controlled Shrinkage of Large-Area Gold Nanoparticle Monolayer Film for Tunable SERS Activity. *Chemistry of Materials* **2018**, *30*, 1989-1997.

23. Fernández-López, C.; Polavarapu, L.; Solís, D. M.; Taboada, J. M.; Obelleiro, F.; Contreras-Cáceres, R.; Pastoriza-Santos, I.; Pérez-Juste, J. Gold Nanorod–pNIPAM Hybrids with Reversible Plasmon Coupling: Synthesis, Modeling, and SERS Properties. *ACS Applied Materials & Interfaces* **2015**, *7*, 12530-12538.

24. Qi, D.; Lu, L.; Wang, L.; Zhang, J. Improved SERS Sensitivity on Plasmon-Free TiO_2 Photonic Microarray by Enhancing Light-Matter Coupling. *Journal of the American Chemical Society* **2014**, *136*, 9886-9889.

25. Zheng, Z.; Cong, S.; Gong, W.; Xuan, J.; Li, G.; Lu, W.; Geng, F.; Zhao, Z. Semiconductor SERS Enhancement Enabled by Oxygen Incorporation. *Nature Communications* **2017**, *8*, 1993.

26. Zhao, B.; Liu, H.; Xia, L.; Wang, Z.; Zhang, C. Gold-Coated Flower-Like TiO_2 Microparticles Wrapped with Reduced Graphene Oxide for SERS Monitoring and Photocatalytic Degradation of Organic Pollutants. *ACS Applied Nano Materials* **2022**, *5*, 15341-15352.

27. Li, J.-F.; Yang, Z.-L.; Ren, B.; Liu, G.-K.; Fang, P.-P.; Jiang, Y.-X.; Wu, D.-Y.; Tian, Z.-Q. Surface-Enhanced Raman Spectroscopy Using Gold-Core Platinum-Shell Nanoparticle Film Electrodes: Toward a Versatile Vibrational Strategy for Electrochemical Interfaces. *Langmuir* **2006**, *22*, 10372-10379.

28. Xie, L.-Q.; Ding, D.; Zhang, M.; Chen, S.; Qiu, Z.; Yan, J.-W.; Yang, Z.-L.; Chen, M.-S.; Mao, B.-W.; Tian, Z.-Q. Adsorption of Dye Molecules on Single Crystalline Semiconductor Surfaces: An Electrochemical Shell-Isolated Nanoparticle Enhanced Raman Spectroscopy Study. *The Journal of Physical Chemistry C* **2016**, *120*, 22500-22507.

29. Kołątaj, K.; Krajczewski, J.; Kudelski, A. Silver Nanoparticles with Many Sharp Apexes and Edges as Efficient Nanoresonators for Shell-Isolated Nanoparticle-Enhanced Raman Spectroscopy. *The Journal of Physical Chemistry C* **2017**, *121*, 12383-12391.

30. Zhang, W.; Yeo, B. S.; Schmid, T.; Zenobi, R. Single Molecule Tip-Enhanced Raman Spectroscopy with Silver Tips. *The Journal of Physical Chemistry C* **2007**, *111*, 1733-1738.

31. Fleischmann, M.; Hendra, P. J.; McQuillan, A. J. Raman Spectra of Pyridine Adsorbed at a Silver Electrode. *Chemical Physics Letters* **1974**, *26*, 163-166.

32. Park, J.-E.; Lee, Y.; Nam, J.-M. Precisely Shaped, Uniformly Formed Gold Nanocubes with Ultrahigh Reproducibility in Single-Particle Scattering and Surface-Enhanced Raman Scattering. *Nano Letters* **2018**, *18*, 6475-6482.

33. Xing, C.; Liu, D.; Chen, J.; Fan, Y.; Zhou, F.; Kaur, K.; Cai, W.; Li, Y. Convective Self-Assembly of 2D Nonclose-Packed Binary Au Nanoparticle Arrays with Tunable Optical Properties. *Chemistry of Materials* **2021**, *33*, 310-319.

34. Zhou, X.; Zhao, Q.; Liu, G.; Zhang, H.; Li, Y.; Cai, W. Temperature Regulation Growth

of Au Nanocrystals: from Concave Trisoctahedron To Dendritic Structures and Their Ultrasensitive SERS-Based Detection of Lindane. *Journal of Materials Chemistry C* **2017**, *5*, 10399-10405.

35. Zhao, Q.; Liu, G.; Zhang, H.; Zhou, F.; Li, Y.; Cai, W. SERS-Based Ultrasensitive Detection of Organophosphorus Nerve Agents via Substrate's Surface Modification. *Journal of Hazardous Materials* **2017**, *324*, 194-202.

36. Liu, D.; Zhou, F.; Li, C.; Zhang, T.; Zhang, H.; Cai, W.; Li, Y. Black Gold: Plasmonic Colloidosomes with Broadband Absorption Self-Assembled from Monodispersed Gold Nanospheres by Using a Reverse Emulsion System. *Angewandte Chemie International Edition* **2015**, *54*, 9596-9600.

37. Zhu, C.; Meng, G.; Zheng, P.; Huang, Q.; Li, Z.; Hu, X.; Wang, X.; Huang, Z.; Li, F.; Wu, N. A Hierarchically Ordered Array of Silver-Nanorod Bundles for Surface-Enhanced Raman Scattering Detection of Phenolic Pollutants. *Advanced Materials* **2016**, *28*, 4871-4876.

38. Huang, Z.; Meng, G.; Huang, Q.; Yang, Y.; Zhu, C.; Tang, C. Improved SERS Performance from Au Nanopillar Arrays by Abridging the Pillar Tip Spacing by Ag Sputtering. *Advanced Materials* **2010**, *22*, 4136-4139.

39. Lin, J.; Shang, Y.; Li, X.; Yu, J.; Wang, X.; Guo, L. Ultrasensitive SERS Detection by Defect Engineering on Single Cu_2O Superstructure Particle. *Advanced Materials* **2017**, *29*, 1604797.

40. Wang, X.; Shi, W.; Jin, Z.; Huang, W.; Lin, J.; Ma, G.; Li, S.; Guo, L. Remarkable SERS Activity Observed from Amorphous ZnO Nanocages. *Angewandte Chemie International Edition* **2017**, *56*, 9851-9855.

41. Zhang, Q.; Li, X.; Ma, Q.; Zhang, Q.; Bai, H.; Yi, W.; Liu, J.; Han, J.; Xi, G. A Metallic Molybdenum Dioxide with High Stability for Surface Enhanced Raman Spectroscopy. *Nature Communications* **2017**, *8*, 14903.

42. Hu, J.-W.; Zhang, Y.; Li, J.-F.; Liu, Z.; Ren, B.; Sun, S.-G.; Tian, Z.-Q.; Lian, T. Synthesis of Au@Pd Core–Shell Nanoparticles with Controllable Size and Their Application in Surface-Enhanced Raman Spectroscopy. *Chemical Physics Letters* **2005**, *408*, 354-359.

43. Tian, Z.-Q.; Ren, B.; Li, J.-F.; Yang, Z.-L. Expanding Generality of Surface-Enhanced Raman Spectroscopy with Borrowing SERS Activity Strategy. *Chemical Communications* **2007**, 3514-3534.

44. Tang, H.; Meng, G.; Huang, Q.; Zhang, Z.; Huang, Z.; Zhu, C. Arrays of Cone-Shaped ZnO Nanorods Decorated with Ag Nanoparticles as 3D Surface-Enhanced Raman Scattering Substrates for Rapid Detection of Trace Polychlorinated Biphenyls. *Advanced Functional Materials* **2012**, *22*, 218-224.

45. Bao, H.; Zhang, H.; Fu, H.; Zhou, L.; Zhang, P.; Li, Y.; Cai, W. Ultrathin Layer Solid Transformation-Enabled-Surface Enhanced Raman Spectroscopy for Trace Harmful Small Gaseous Molecule Detection. *Nanoscale Horizons* **2020**, *5*, 739-746.

46. Xie, W.; Walkenfort, B.; Schlücker, S. Label-Free SERS Monitoring of Chemical Reactions Catalyzed by Small Gold Nanoparticles Using 3D Plasmonic Superstructures. *Journal of the American Chemical Society* **2013**, *135*, 1657-1660.

47. Zhang, H.; Wang, C.; Sun, H.-L.; Fu, G.; Chen, S.; Zhang, Y.-J.; Chen, B.-H.; Anema, J. R.; Yang, Z.-L.; Li, J.-F.; Tian, Z.-Q. In Situ Dynamic Tracking of Heterogeneous Nanocatalytic Processes by Shell-Isolated Nanoparticle-Enhanced Raman Spectroscopy. *Nature Communications* **2017**, *8*, 15447.

48. Zhang, Y.-J.; Ze, H.; Fang, P.-P.; Huang, Y.-F.; Kudelski, A.; Fernández-Vidal, J.; Hardwick, L. J.; Lipkowski, J.; Tian, Z.-Q.; Li, J.-F. Shell-isolated nanoparticle-enhanced Raman spectroscopy. *Nature Reviews Methods Primers* **2023**, *3*, 36.

49. Stöckle, R. M.; Suh, Y. D.; Deckert, V.; Zenobi, R. Nanoscale Chemical Analysis by Tip-Enhanced Raman Spectroscopy. *Chemical Physics Letters* **2000**, *318*, 131-136.

50. Pettinger, B.; Picardi, G.; Schuster, R.; Ertl, G. Surface Enhanced Raman Spectroscopy: Towards Single Molecule Spectroscopy. *Electrochemistry* **2000**, *68*, 942-949.

51. Lu, G.; Li, H.; Zhang, H. Nanoparticle-Coated PDMS Elastomers for Enhancement of Raman Scattering. *Chemical Communications* **2011**, *47*, 8560-8562.

52. Zhang, Z.; Sheng, S.; Wang, R.; Sun, M. Tip-Enhanced Raman Spectroscopy. *Analytical Chemistry* **2016**, *88*, 9328-9346.

53. Zhang, K.; Yang, L.; Hu, Y.; Fan, C.; Zhao, Y.; Bai, L.; Li, Y.; Shi, F.; Liu, J.; Xie, W. Synthesis of a Gold–Metal Oxide Core–Satellite Nanostructure for In Situ SERS Study of CuO-Catalyzed Photooxidation. *Angewandte Chemie International Edition* **2020**, *59*, 18003-18009.

54. Wang, Y.-H.; Zheng, S.; Yang, W.-M.; Zhou, R.-Y.; He, Q.-F.; Radjenovic, P.; Dong, J.-C.; Li, S.; Zheng, J.; Yang, Z.-L.; Attard, G.; Pan, F.; Tian, Z.-Q.; Li, J.-F. In Situ Raman Spectroscopy Reveals the Structure and Dissociation of Interfacial Water. *Nature* **2021**, *600*, 81-85.

55. Dong, J.-C.; Su, M.; Briega-Martos, V.; Li, L.; Le, J.-B.; Radjenovic, P.; Zhou, X.-S.; Feliu, J. M.; Tian, Z.-Q.; Li, J.-F. Direct In Situ Raman Spectroscopic Evidence of Oxygen Reduction Reaction Intermediates at High-Index Pt(hkl) Surfaces. *Journal of the American Chemical Society* **2020**, *142*, 715-719.

56. Galloway, T. A.; Dong, J.-C.; Li, J.-F.; Attard, G.; Hardwick, L. J. Oxygen reactions on Pt{hkl} in a non-aqueous Na^+ electrolyte: site selective stabilisation of a sodium peroxy species. *Chemical Science* **2019**, *10*, 2956-2964.

57. Dong, J.-C.; Zhang, X.-G.; Briega-Martos, V.; Jin, X.; Yang, J.; Chen, S.; Yang, Z.-L.; Wu, D.-Y.; Feliu, J. M.; Williams, C. T.; Tian, Z.-Q.; Li, J.-F. In Situ Raman Spectroscopic Evidence for Oxygen Reduction Reaction Intermediates at Platinum Single-Crystal Surfaces. *Nature Energy* **2019**, *4*, 60-67.

58. Kang, L.; Guo, Y.; Miao, P.; Sun, M.; Song, B.; Xu, P.; Liu, X. Study of Surface Plasmon Assisted Reactions to Understand the Light-Induced Decarboxylation of N719 Sensitizer. *European Journal of Inorganic Chemistry* **2019**, *2019*, 23-28.

59. Gajan, A.; Lecourt, C.; Torres Bautista, B. E.; Fillaud, L.; Demeaux, J.; Lucas, I. T. Solid Electrolyte Interphase Instability in Operating Lithium-Ion Batteries Unraveled by Enhanced-Raman Spectroscopy. *ACS Energy Letters* **2021**, *6*, 1757-1763.

60. Glass, D.; Cortés, E.; Ben-Jaber, S.; Brick, T.; Peveler, W. J.; Blackman, C. S.; Howle, C. R.; Quesada-Cabrera, R.; Parkin, I. P.; Maier, S. A. Dynamics of Photo-Induced Surface Oxygen Vacancies in Metal-Oxide Semiconductors Studied Under Ambient Conditions. *Advanced Science* **2019**, *6*, 1901841.

61. Glass, D.; Quesada-Cabrera, R.; Bardey, S.; Promdet, P.; Sapienza, R.; Keller, V.; Maier, S. A.; Caps, V.; Parkin, I. P.; Cortés, E. Probing the Role of Atomic Defects in Photocatalytic Systems through Photoinduced Enhanced Raman Scattering. *ACS Energy Letters* **2021**, *6*, 4273-4281.

62. Huang, J.; Niu, W.; Li, C.; Tan, C.; Yin, P.; Cheng, H.; Hu, Z.; Yang, N.; He, Q.; Nam, G.-H.; Zhang, H. In-Situ Probing of Crystal-Phase-Dependent Photocatalytic Activities of Au Nanostructures by Surface-Enhanced Raman Spectroscopy. *ACS Materials Letters* **2020**, *2*, 409-414.

63. Zhan, C.; Wang, Z.-Y.; Zhang, X.-G.; Chen, X.-J.; Huang, Y.-F.; Hu, S.; Li, J.-F.; Wu, D.-Y.; Moskovits, M.; Tian, Z.-Q. Interfacial Construction of Plasmonic Nanostructures for the Utilization of the Plasmon-Excited Electrons and Holes. *Journal of the American Chemical Society* **2019**, *141*, 8053-8057.

64. Cai, Z.-F.; Merino, J. P.; Fang, W.; Kumar, N.; Richardson, J. O.; De Feyter, S.; Zenobi, R. Molecular-Level Insights on Reactive Arrangement in On-Surface Photocatalytic Coupling Reactions Using Tip-Enhanced Raman Spectroscopy. *Journal of the American Chemical Society* **2022**, *144*, 538-546.

65. Devasia, D.; Wilson, A. J.; Heo, J.; Mohan, V.; Jain, P. K. A Rich Catalog of C–C Bonded Species Formed in CO_2 Reduction on a Plasmonic Photocatalyst. *Nature Communications* **2021**, *12*, 2612.

66. Kumari, G.; Zhang, X.; Devasia, D.; Heo, J.; Jain, P. K. Watching Visible Light-Driven CO_2 Reduction on a Plasmonic Nanoparticle Catalyst. *ACS Nano* **2018**, *12*, 8330-8340.

67. Hu, C.; Hu, Y.; Fan, C.; Yang, L.; Zhang, Y.; Li, H.; Xie, W. Surface-Enhanced Raman

Spectroscopic Evidence of Key Intermediate Species and Role of NiFe Dual-Catalytic Center in Water Oxidation. *Angewandte Chemie International Edition* **2021**, *60*, 19774-19778.

68. An, H.; Wu, L.; Mandemaker, L. D. B.; Yang, S.; de Ruiter, J.; Wijten, J. H. J.; Janssens, J. C. L.; Hartman, T.; van der Stam, W.; Weckhuysen, B. M. Sub-Second Time-Resolved Surface-Enhanced Raman Spectroscopy Reveals Dynamic CO Intermediates during Electrochemical CO_2 Reduction on Copper. *Angewandte Chemie International Edition* **2021**, *60*, 16576-16584.

69. de Ruiter, J.; An, H.; Wu, L.; Gijsberg, Z.; Yang, S.; Hartman, T.; Weckhuysen, B. M.; van der Stam, W. Probing the Dynamics of Low-Overpotential CO_2-to-CO Activation on Copper Electrodes with Time-Resolved Raman Spectroscopy. *Journal of the American Chemical Society* **2022**, *144*, 15047-15058.

70. Yao, D.; Tang, C.; Li, L.; Xia, B.; Vasileff, A.; Jin, H.; Zhang, Y.; Qiao, S.-Z. In Situ Fragmented Bismuth Nanoparticles for Electrocatalytic Nitrogen Reduction. *Advanced Energy Materials* **2020**, *10*, 2001289.

71. He, L.; Zhang, W.; Mo, Q.; Huang, W.; Yang, L.; Gao, Q. Molybdenum Carbide-Oxide Heterostructures: In Situ Surface Reconfiguration toward Efficient Electrocatalytic Hydrogen Evolution. *Angewandte Chemie International Edition* **2020**, *59*, 3544-3548.

72. Shan, W.; Liu, R.; Zhao, H.; He, Z.; Lai, Y.; Li, S.; He, G.; Liu, J. In Situ Surface-Enhanced Raman Spectroscopic Evidence on the Origin of Selectivity in CO_2 Electrocatalytic Reduction. *ACS Nano* **2020**, *14*, 11363-11372.

73. Koh, C. S. L.; Lee, H. K.; Fan Sim, H. Y.; Han, X.; Phan-Quang, G. C.; Ling, X. Y. Turning Water from a Hindrance to the Promotor of Preferential Electrochemical Nitrogen Reduction. *Chemistry of Materials* **2020**, *32*, 1674-1683.

74. Zhong, H.-L.; Ze, H.; Zhang, X.-G.; Zhang, H.; Dong, J.-C.; Shen, T.; Zhang, Y.-J.; Sun, J.-J.; Li, J.-F. In Situ SERS Probing the Effect of Additional Metals on Pt-Based Ternary Alloys toward Improving ORR Performance. *ACS Catalysis* **2023**, *13*, 6781-6786.

75. Lin, X.-M.; Wang, X.-T.; Deng, Y.-L.; Chen, X.; Chen, H.-N.; Radjenovic, P. M.; Zhang, X.-G.; Wang, Y.-H.; Dong, J.-C.; Tian, Z.-Q.; Li, J.-F. In Situ Probe of the Hydrogen Oxidation Reaction Intermediates on PtRu a Bimetallic Catalyst Surface by Core–Shell Nanoparticle-Enhanced Raman Spectroscopy. *Nano Letters* **2022**, *22*, 5544-5552.

76. Wang, Y. H.; Wang, X. T.; Ze, H.; Zhang, X. G.; Radjenovic, P. M.; Zhang, Y. J.; Dong, J. C.; Tian, Z. Q.; Li, J. F. Spectroscopic Verification of Adsorbed Hydroxy Intermediates in the Bifunctional Mechanism of the Hydrogen Oxidation Reaction. *Angewandte Chemie* **2021**, *133*, 5772-5775.

77. Chen, H. Q.; Ze, H.; Yue, M. F.; Wei, D. Y.; Wu, Y. F.; Dong, J. C.; Zhang, Y. J.; Zhang, H.; Tian, Z. Q.; Li, J. F. Unmasking the Critical Role of the Ordering Degree of Bimetallic

Nanocatalysts on Oxygen Reduction Reaction by in Situ Raman Spectroscopy. *Angewandte Chemie* **2022**, *134*, e202117834.

78. Liu, J.; Zhong, H.-L.; Li, X.; Yue, M.-F.; Yang, W.-M.; You, X.; Tian, J.-H.; Wang, Y.-H.; Li, J.-F. Core-Shell Nanoparticle Enhanced Raman Spectroscopy in Situ Probing the Composition and Evolution of Interfacial Species on PtCo Surfaces. *Nano Research* **2023**.

79. Li, X.; Blinn, K.; Chen, D.; Liu, M. In Situ and Surface-Enhanced Raman Spectroscopy Study of Electrode Materials in Solid Oxide Fuel Cells. *Electrochemical Energy Reviews* **2018**, *1*, 433-459.

80. Kim, J. H.; Chern, Z.-Y.; Yoo, S.; deGlee, B.; Wang, J.; Liu, M. Unraveling the Mechanism of Water-Mediated Sulfur Tolerance via Operando Surface-Enhanced Raman Spectroscopy. *ACS Applied Materials & Interfaces* **2020**, *12*, 2370-2379.

81. Su, Y.; Wei, T.; Li, Y.; Yin, B.; Huan, Y.; Dong, D.; Hu, X.; Huang, B. A Highly Active CH_4 Catalyst Correlated with Solid Oxide Fuel Cell Anode Performance. *Journal of Materials Chemistry A* **2021**, *9*, 5067-5074.

82. Zhang, S.-P.; Lin, J.-S.; Lin, R.-K.; Radjenovic, P. M.; Yang, W.-M.; Xu, J.; Dong, J.-C.; Yang, Z.-L.; Hang, W.; Tian, Z.-Q.; Li, J.-F. In Situ Raman Study of the Photoinduced Behavior of Dye Molecules on TiO_2(hkl) Single Crystal Surfaces. *Chemical Science* **2020**, *11*, 6431-6435.

83. Zhu, L.; Li, P.; Sun, H.; Han, X.; Xu, Y.; Wang, X.; Liu, B.; Ozaki, Y.; Zhao, B. An Investigation of the Effect of High-Pressure on Charge Transfer in Dye-Sensitized Solar Cells based on Surface-Enhanced Raman Spectroscopy. *Nanoscale* **2022**, *14*, 373-381.

84. Wang, X.; Han, X. X.; Ma, H.; Li, P.; Li, X.; Kitahama, Y.; Zhao, B.; Ozaki, Y. Reduced Charge-Transfer Threshold in Dye-Sensitized Solar Cells with an Au@Ag/N3/n-TiO_2 Structure As Revealed by Surface-Enhanced Raman Scattering. *The Journal of Physical Chemistry C* **2018**, *122*, 12748-12760.

85. Wang, X.; Li, P.; Han, X. X.; Kitahama, Y.; Zhao, B.; Ozaki, Y. An Enhanced Degree of Charge Transfer in Dye-Sensitized Solar Cells with a ZnO-TiO_2/N3/Ag Structure as Revealed by Surface-Enhanced Raman Scattering. *Nanoscale* **2017**, *9*, 15303-15313.

86. Zhao, Z.; Zhang, X.; Zhou, Z.; Wang, E.; Peng, Z. Direct In Situ Spectroscopic Evidence for Solution-Mediated Oxygen Reduction Reaction Intermediates in Aprotic Lithium–Oxygen Batteries. *Nano Letters* **2022**, *22*, 501-507.

87. Qiao, Y.; Yang, H.; Chang, Z.; Deng, H.; Li, X.; Zhou, H. A High-Energy-Density and Long-Life Initial-Anode-Free Lithium Battery Enabled by a Li_2O Sacrificial Agent. *Nature Energy* **2021**, *6*, 653-662.

88. Chen, D.; Mahmoud, M. A.; Wang, J.-H.; Waller, G. H.; Zhao, B.; Qu, C.; El-Sayed, M. A.; Liu, M. Operando Investigation into Dynamic Evolution of Cathode–Electrolyte Interfaces

in a Li-Ion Battery. *Nano Letters* **2019**, *19*, 2037-2043.

89. Martín-Yerga, D.; Milan, D. C.; Xu, X.; Fernández-Vidal, J.; Whalley, L.; Cowan, A. J.; Hardwick, L. J.; Unwin, P. R. Dynamics of Solid-Electrolyte Interphase Formation on Silicon Electrodes Revealed by Combinatorial Electrochemical Screening. *Angewandte Chemie International Edition* **2022**, *61*, e202207184.

90. Gu, Y.; You, E.-M.; Lin, J.-D.; Wang, J.-H.; Luo, S.-H.; Zhou, R.-Y.; Zhang, C.-J.; Yao, J.-L.; Li, H.-Y.; Li, G.; Wang, W.-W.; Qiao, Y.; Yan, J.-W.; Wu, D.-Y.; Liu, G.-K.; Zhang, L.; Li, J.-F.; Xu, R.; Tian, Z.-Q.; Cui, Y.; Mao, B.-W. Resolving Nanostructure and Chemistry of Solid-Electrolyte Interphase on Lithium Anodes by Depth-Sensitive Plasmon-Enhanced Raman Spectroscopy. *Nature Communications* **2023**, *14*, 3536.

91. Zhang, R.; Zhang, Y.; Dong, Z. C.; Jiang, S.; Zhang, C.; Chen, L. G.; Zhang, L.; Liao, Y.; Aizpurua, J.; Luo, Y.; Yang, J. L.; Hou, J. G. Chemical Mapping of a Single Molecule by Plasmon-Enhanced Raman Scattering. *Nature* **2013**, *498*, 82-86.

92. Kumar, N.; Weckhuysen, B. M.; Wain, A. J.; Pollard, A. J. Nanoscale Chemical Imaging Using Tip-Enhanced Raman Spectroscopy. *Nature Protocols* **2019**, *14*, 1169-1193.

93. Van Schrojenstein Lantman, E. M.; Deckert-Gaudig, T.; Mank, A. J. G.; Deckert, V.; Weckhuysen, B. M. Catalytic Processes Monitored at the Nanoscale with Tip-Enhanced Raman Spectroscopy. *Nature Nanotechnology* **2012**, *7*, 583-586.

94. Lee, J.; Crampton, K. T.; Tallarida, N.; Apkarian, V. A. Visualizing Vibrational Normal Modes of a Single Molecule with Atomically Confined Light. *Nature* **2019**, *568*, 78-82.

95. Warkentin, C. L.; Yu, Z.; Sarkar, A.; Frontiera, R. R. Decoding Chemical and Physical Processes Driving Plasmonic Photocatalysis Using Surface-Enhanced Raman Spectroscopies. *Accounts of Chemical Research* **2021**, *54*, 2457-2466.

96. Kim, J. Y.; Lee, J.-W.; Jung, H. S.; Shin, H.; Park, N.-G. High-Efficiency Perovskite Solar Cells. *Chemical Reviews* **2020**, *120*, 7867-7918.

97. Omar, A.; Ali, M. S.; Abd Rahim, N. Electron Transport Properties Analysis of Titanium Dioxide Dye-Sensitized Solar Cells (TiO_2-DSSCS) Based Natural Dyes Using Electrochemical Impedance Spectroscopy Concept: A Review. *Solar Energy* **2020**, *207*, 1088-1121.

98. Li, X.; McNaughter, P. D.; O'Brien, P.; Minamimoto, H.; Murakoshi, K. Photoelectrochemical Formation of Polysulfide at PbS QD-Sensitized Plasmonic Electrodes. *The Journal of Physical Chemistry Letters* **2019**, *10*, 5357-5363.

99. Wang, Y.; Liu, J.; Ozaki, Y.; Xu, Z.; Zhao, B. Effect of TiO_2 on Altering Direction of Interfacial Charge Transfer in a TiO_2-Ag-MPY-FePc System by SERS. *Angewandte Chemie International Edition* **2019**, *58*, 8172-8176.

100. Zang, Y.; Liu, T.; Wei, P.; Li, H.; Wang, Q.; Wang, G.; Bao, X. Selective CO_2

Electroreduction to Ethanol over a Carbon-Coated CuO_x Catalyst. *Angewandte Chemie International Edition* **2022**, *61*, e202209629.

101. Hasa, B.; Zhao, Y.; Jiao, F. In Situ/Operando Characterization Techniques of Electrochemical CO_2 Reduction. *Annual Review of Chemical and Biomolecular Engineering* **2023**, *14*, 165-185.

102. Zhu, P.; Xia, C.; Liu, C.-Y.; Jiang, K.; Gao, G.; Zhang, X.; Xia, Y.; Lei, Y.; Alshareef, H. N.; Senftle, T. P.; Wang, H. Direct and Continuous Generation of Pure Acetic Acid Solutions via Electrocatalytic Carbon Monoxide Reduction. *Proceedings of the National Academy of Sciences of the United States of America* **2021**, *118*, e2010868118.

103. Chen, J.; Ma, B.; Xie, Z.; Li, W.; Yang, Y.; Mu, M.; Zou, X.; Zhao, B.; Song, W. Bifunctional porous SnO_2/Ag nanofibers for efficient electroreduction of carbon dioxide to formate and its mechanism elucidation by in-situ surface-enhanced Raman scattering. *Applied Catalysis B: Environmental* **2023**, *325*, 122350.

104. Boldrin, P.; Brandon, N. P. Progress and Outlook for Solid Oxide Fuel Cells for Transportation Applications. *Nature Catalysis* **2019**, *2*, 571-577.

105. Sun, Y.-L.; A, Y.-L.; Yue, M.-F.; Chen, H.-Q.; Ze, H.; Wang, Y.-H.; Dong, J.-C.; Tian, Z.-Q.; Fang, P.-P.; Li, J.-F. Exploring the Effect of Pd on the Oxygen Reduction Performance of Pt by In Situ Raman Spectroscopy. *Analytical Chemistry* **2022**, *94*, 4779-4786.

106. Chen, Y.; Yoo, S.; Li, X.; Ding, D.; Pei, K.; Chen, D.; Ding, Y.; Zhao, B.; Murphy, R.; deGlee, B.; Liu, J.; Liu, M. An Effective Strategy to Enhancing Tolerance to Contaminants Poisoning of Solid Oxide Fuel Cell Cathodes. *Nano Energy* **2018**, *47*, 474-480.

107. Kim, J. H.; Liu, M.; Chen, Y.; Murphy, R.; Choi, Y.; Liu, Y.; Liu, M. Understanding the Impact of Sulfur Poisoning on the Methane-Reforming Activity of a Solid Oxide Fuel Cell Anode. *ACS Catalysis* **2021**, *11*, 13556-13566.

108. Zhou, G.; Mo, L.; Zhou, C.; Wu, Y.; Lai, F.; Lv, Y.; Ma, J.; Miao, Y.-E.; Liu, T. Ultra-Strong Capillarity of Bioinspired Micro/Nanotunnels in Organic Cathodes Enabled High-Performance All-Organic Sodium-Ion Full Batteries. *Chemical Engineering Journal* **2021**, *420*, 127597.

109. Kuang, Y.; Chen, C.; Kirsch, D.; Hu, L. Thick Electrode Batteries: Principles, Opportunities, and Challenges. *Advanced Energy Materials* **2019**, *9*, 1901457.

110. Li, Y.; Wang, Z.; Cai, Y.; Pam, M. E.; Yang, Y.; Zhang, D.; Wang, Y.; Huang, S. Designing Advanced Aqueous Zinc-Ion Batteries: Principles, Strategies, and Perspectives. *Energy Environ. Mater.* **2022**, *5*, 823-851.

111. He, Q.-F.; Zhang, Y.-J.; Yang, Z.-L.; Dong, J.-C.; Lin, X.-M.; Li, J.-F. Surface-Enhanced Raman Spectroscopy: Principles, Methods, and Applications in Energy Systems. *Chinese*

Journal of Chemistry **2023**, *41*, 355-369.

112. Zang, Y.; Zhang, H.; Zhang, X.; Liu, R.; Liu, S.; Wang, G.; Zhang, Y.; Zhao, H. Fe/Fe_2O_3 Nanoparticles Anchored on Fe-N-Doped Carbon Nanosheets as Bifunctional Oxygen Electrocatalysts for Rechargeable Zinc-Air Batteries. *Nano Research* **2016**, *9*, 2123-2137.

113. Wang, J.; Ma, L.; Xu, J.; Xu, Y.; Sun, K.; Peng, Z. Oxygen Electrochemistry in Li-O_2 Batteries Probed by in situ Surface-Enhanced Raman Spectroscopy. *SusMat* **2021**, *1*, 345-358.

114. Leong, Y. X.; Tan, E. X.; Leong, S. X.; Lin Koh, C. S.; Thanh Nguyen, L. B.; Ting Chen, J. R.; Xia, K.; Ling, X. Y. Where Nanosensors Meet Machine Learning: Prospects and Challenges in Detecting Disease X. *ACS Nano* **2022**, *16*, 13279-13293.

115. Leong, S. X.; Leong, Y. X.; Koh, C. S. L.; Tan, E. X.; Nguyen, L. B. T.; Chen, J. R. T.; Chong, C.; Pang, D. W. C.; Sim, H. Y. F.; Liang, X.; Tan, N. S.; Ling, X. Y. Emerging Nanosensor Platforms and Machine Learning Strategies toward Rapid, Point-of-Need Small-Molecule Metabolite Detection and Monitoring. *Chemical Science* **2022**, *13*, 11009-11029.

116. Gruenke, N. L.; Cardinal, M. F.; McAnally, M. O.; Frontiera, R. R.; Schatz, G. C.; Van Duyne, R. P. Ultrafast and Nonlinear Surface-Enhanced Raman Spectroscopy. *Chemical Society Reviews* **2016**, *45*, 2263-2290.

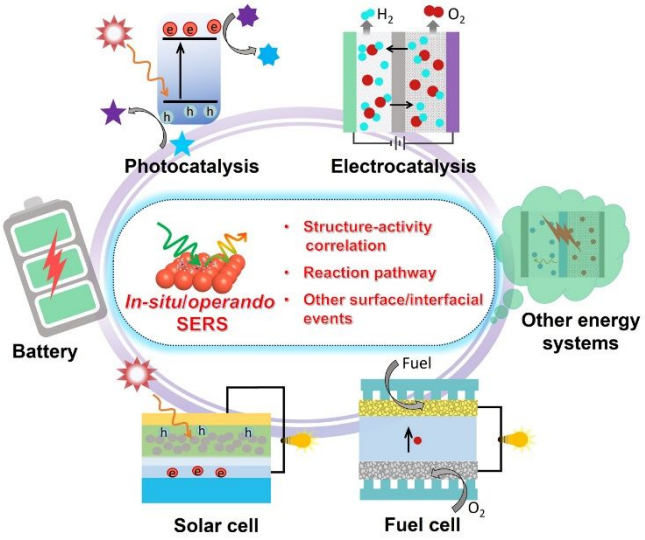

TOC